Cytokinin receptor AHK3 influences leaf size by modulating *trans*-zeatin-type cytokinin levels in xylem

Kota Monden[a†], Takamasa Suzuki[b], Mikiko Kojima[c], Yumiko Takebayashi[c], Takehiro Kamiya[d], Takatoshi Kiba[e,f], Hitoshi Sakakibara[c,f], Tsuyoshi Nakagawa[a], and Takushi Hachiya[a]

[a]Department of Molecular and Functional Genomics, Interdisciplinary Center for Science Research, Shimane University, 1060 Nishikawatsu-cho, Matsue, Shimane 690-8504, Japan

[b]College of Bioscience and Biotechnology, Chubu University, 1200 Matsumoto-cho, Kasugai, Aichi 487-8501, Japan

[c]RIKEN Center for Sustainable Resource Science, 1-7-22 Suehiro-cho, Tsurumi-ku, Yokohama, Kanagawa 230-0045, Japan

[d]Graduate School of Agricultural and Life Sciences, Tokyo University, 1-1-1 Yayoi, Bunkyo-ku, Tokyo 113-8657, Japan

[e]Institute of Plant Science and Resources, Okayama University, 2-20-1 Chuo, Kurashiki, Okayama 710-0046, Japan

[f]Graduate School of Bioagricultural Sciences, Nagoya University, Furo-cho, Chikusa-ku, Nagoya, Aichi 464-8601, Japan

[†] **To whom correspondence should be addressed.**

Kota Monden

Email: n23d203@matsu.shimane-u.ac.jp

Tel.: +81-852-32-6288

SUMMARY

Trans-zeatin (*t*Z)-type cytokinins (CKs) are synthesized in roots in response to nitrate, transported to shoot via xylem, and coordinate diverse physiological processes in aerial organs. Within this mechanism, the regulation of CK biosynthesis by nitrate signaling via NIN-like protein 7 as well as the loading of *t*Z-type CKs into xylem by ATP-binding cassette transporter G14 have been well studied. However, the roles of other components remain unclear. Here, we show that CK perception and degradation in roots, as mediated by Arabidopsis histidine kinase 3 (AHK3) and CK oxidase/dehydrogenase 4 (CKX4), modulate xylem *t*Z-type CKs transport and leaf CK status. Grafting experiments demonstrated that root-specific *AHK3* deficiency systemically increased leaf blade area through long-distance signals of root-derived *t*Z-type CK, perceived by shoot-expressed AHK3. Transcriptome and hormonome analyses revealed that root-specific *AHK3* deficiency reduced *CKX4* expression in roots, elevating *t*Z-type CK levels in roots and xylem sap and thereby enhancing leaf CK response. Transfer experiments manipulating root nitrate levels showed that root-specific *AHK3* deficiency promoted leaf blade area in a manner dependent on both nitrate and root-derived *t*Z-type CK signaling. Moreover, both nitrate signals and root-expressed AHK3 are required for maximal *CKX4* induction in roots, and root-specific *CKX4* deficiency enhanced leaf blade area in a nitrate-dependent manner. These findings reveal a novel mechanism in which an AHK3–CKX4 module governs xylem transport of *t*Z-type CKs, fine-tuning leaf size according to nitrogen availability in roots.

Keywords:

cytokinin; *trans*-zeatin; nitrate signal; micrografting; *Arabidopsis thaliana*

49 **SIGNIFICANCE STATEMENT**

50 To clarify a mechanism that attenuates *trans*-zeatin-type cytokinin transport from roots
51 to shoots in response to nitrate signaling, this study examined the root-specific role of
52 cytokinin receptors. Our results show that cytokinin perception and degradation, as
53 mediated by Arabidopsis histidine kinase 3 and cytokinin oxidase/dehydrogenase 4,
54 modulate xylem *trans*-zeatin-type cytokinin transport, thereby fine-tuning leaf cytokinin
55 status and growth in a nitrate-dependent manner, providing new insights into long-
56 distance cytokinin transport according to nitrogen availability.

57

58 **INTRODUCTION**

59 Cytokinins (CKs) are essential plant hormones that coordinate diverse developmental and
60 physiological processes, including cell division, shoot and root growth, vascular
61 formation, and responses to stress and nutrients (Werner et al., 2001; Riefler et al., 2006;
62 Matsumoto-Kitano et al., 2008; Sakakibara, 2021). In *Arabidopsis*, the biologically active
63 CK forms include N^6-(Δ^2-isopentenyl) adenine (iP) and *trans*-zeatin (*t*Z). The initial and
64 rate-limiting step of CK biosynthesis involves N^6-prenylation of adenosine 5′-phosphates
65 catalyzed by adenosine phosphate-isopentenyltransferases (IPTs), producing iP-riboside
66 5′-phosphates (iPRPs) (Takei et al., 2001a; Miyawaki et al., 2006). These intermediates
67 are subsequently hydroxylated by cytochrome P450 monooxygenases CYP735A1 and
68 CYP735A2 to form *t*Z-riboside 5′-phosphates (*t*ZRPs) (Takei et al., 2004a). Ribotide
69 precursors are then converted into iP and *t*Z by CK-activating enzyme members of the
70 lonely guy (LOG) family (Kurakawa et al., 2007; Kuroha et al., 2009). CK homeostasis
71 is further modulated by reversible *O*-glucosylation and tentatively reversible *N*-
72 glucosylation catalyzed by glucosyltransferases (UGTs), and by irreversible degradation

73 by cytokinin oxidase/dehydrogenases (CKXs) (Werner et al., 2006; Wang et al., 2011;
74 Jin et al., 2013; Wang et al., 2013; Hošek et al., 2020). CK perception and signaling rely
75 on a multistep His-to-Asp phosphorelay system (Hutchison and Kieber, 2002; Müller and
76 Sheen, 2007). Three membrane-spanning histidine kinases, Arabidopsis histidine kinase
77 (AHK)2, AHK3, and CRE1/AHK4, act as CK receptors (Inoue et al., 2001). Upon ligand
78 binding, the phosphoryl group is transferred from AHKs to histidine phosphotransfer
79 proteins, which shuttle into the nucleus and activate type-B response regulators
80 (Hutchison and Kieber, 2002; Müller and Sheen, 2007). These transcription factors
81 induce CK-responsive genes, including type-A response regulators that function as
82 negative feedback elements (To et al., 2004).

83 In addition to local roles, CKs act as long-distance signaling molecules that
84 coordinate developmental and physiological processes between roots and shoots
85 (Sakakibara, 2021). In *Arabidopsis*, *t*Z-type CKs predominate in xylem sap, whereas iP-
86 type CKs are more abundant in phloem sap (Hirose et al., 2008; Osugi et al., 2017). This
87 distribution reflects tissue-specific expression of CK biosynthetic genes: *CYP735A2* is
88 strongly expressed in root vasculature, while *IPT3* is mainly expressed in phloem tissues
89 of both roots and shoots (Miyawaki et al., 2004; Takei et al., 2004a,b; Kiba et al., 2013).
90 These activities establish a directional flow of CK species, with root-derived *t*Z-type CKs
91 transported to shoots via xylem and shoot-derived iP-type CKs transported to roots via
92 phloem tissue (Hirose et al., 2008; Matsumoto-Kitano et al., 2008; Kiba et al., 2013). A
93 central component of the root-to-shoot CK transport system is ATP-binding cassette
94 transporter G14 (ABCG14), which loads CKs into xylem in root stele and also contributes
95 to phloem unloading in shoots (Ko et al., 2014; Zhang et al., 2014; Zhao et al., 2021).
96 Importantly, root-to-shoot transport of *t*Z-type CKs mediated by ABCG14 is essential for

97 maintaining shoot growth, which is supported by the observation that *abcg14* mutants
98 show strongly reduced shoot growth during both the vegetative and reproductive stages
99 (Ko et al., 2014; Zhang et al., 2014). In addition, heterologous transport assays in yeast
100 have shown that ABCG14 transports multiple CK species, including both iP- and *t*Z-types,
101 underscoring its pivotal role in systemic CK distribution and signaling (Zhao et al., 2023).
102 Root-to-shoot *t*Z-type CK transport is strongly influenced by plant nitrogen
103 status. In *Arabidopsis*, nitrate supply induces the expression of *IPT3* and *CYP735A2* in
104 roots and increases the concentrations of *t*ZR and *t*ZRMP (Takei et al., 2004b; Maeda et
105 al., 2018). Nitrate supply also enhances the xylem transport of *t*Z-riboside (*t*ZR) and
106 activation of CK signaling in leaves (Sakakibara et al., 1998; Takei et al., 2001b; Osugi
107 et al., 2017; Abualia et al., 2022). Furthermore, NIN-like protein 7 (NLP7), a nitrate
108 sensor, drives the nitrate-dependent induction of *IPT3* and *CYP735A2* (Liu et al., 2022).
109 Therefore, nitrate-induced increases in *t*Z and *t*ZR concentrations and in *ARR5* promoter
110 activity in shoots are markedly reduced in *nlp7* mutants (Abualia et al., 2022). Nitrate
111 signaling also induces *ABCG14* expression in roots in an NLP7-dependent manner
112 (Abualia et al., 2022). In addition, long-distance signals of root-derived *t*Z and *t*ZR
113 differentially affect leaf growth traits, and their ratios in xylem sap are known to be
114 modulated by nitrate supply (Osugi et al., 2017). Taken together, these findings indicate
115 that plants adjust leaf growth according to root nitrate status mediated by *t*Z-type CKs,
116 and that NLP7 and ABCG14 act as key components governing the root-to-shoot transport
117 of *t*Z-type CKs. On the other hand, the feedback mechanism that attenuates the nitrate-
118 induced accumulation of *t*Z-type CKs remains poorly understood. The nitrate-inducible
119 GARP-type transcriptional repressor 1s (NIGT1s) are induced by NLPs and repress *IPT3*
120 and *CYP735A2* expression, suggesting that they may function as feedback components

121 (Kiba et al., 2018; Maeda et al., 2018). However, because *nigt1.1/1.2/1.3/1.4* quadruple
122 mutants show only a modest increase in *t*Z-type CK concentrations (Maeda et al., 2018),
123 other major feedback components that modulate *t*Z-type CK levels likely remain
124 unidentified.

125 One promising candidate for a key feedback component may be AHK3. In
126 *Arabidopsis*, disruption of *AHK3* causes a pronounced twofold to threefold increase in all
127 *t*Z-type CK species (Riefler et al., 2006). Moreover, our previous study proposed that
128 root-specific deficiencies of *AHK2* and *AHK3* increased *t*Z-type CKs concentration in
129 roots, which in turn affected *t*Z-type CKs concentrations, type-A *ARRs* expressions, and
130 growth in the shoot (Monden et al., 2022). Furthermore, *AHK3* was identified as one of
131 the top genes co-expressed with *NLP7* (Supplementary Table S1), suggesting that AHK3
132 may act in association with nitrate responses via NLP7. In addition, AHK3 has been
133 reported to exhibit a higher affinity for *t*Z than for iP (Stolz et al., 2011), implying a
134 preferential role in *t*Z-type CK signaling. Together, these findings suggest that root-
135 expressed AHK3 may modulate root-to-shoot transport of *t*Z-type CKs in response to
136 nitrogen availability in roots, although the underlying mechanism and physiological
137 relevance remain unclear.

138 In this study, we show that CK perception and degradation in roots, mediated
139 by AHK3 and CKX4, modulate *t*Z-type CK levels in the xylem, thereby influencing CK
140 responses and growth in leaves. Growth analyses of grafted plants demonstrated that root-
141 specific *AHK3* deficiency enlarged leaf blade area through long-distance signals of root-
142 derived *t*Z-type CK, perceived by shoot-expressed AHK3. Transcriptome and
143 hormonome analysis further revealed that root-specific *AHK3* deficiency reduced *CKX4*
144 expression in roots, elevating *t*Z-type CK levels in roots and xylem sap and thereby

145 enhancing CK responses in leaves. Transfer experiments manipulating root nitrate levels
146 showed that nitrate-induced leaf growth promotion depends on long-distance signals of
147 root-derived *t*Z-type CK, which is in turn controlled by root-expressed AHK3 and CKX4.
148 We propose a mechanism in which the AHK3–CKX4 module governs xylem transport
149 of *t*Z-type CK in response to nitrogen availability in roots, thereby fine-tuning leaf size
150 to maintain balanced plant growth.
151

152 **RESULTS**

153 **Root-expressed AHK3 modulates shoot and root growth**

154 To identify which root-expressed CK receptor(s) influence shoot and root growth, we
155 grafted Col-0 (WT) scions onto rootstocks derived from WT, single mutant (i.e., *ahk2-5*;
156 *ahk2*, *ahk3-7*; *ahk3*, *cre1-2*; *ahk4*) or double mutant (i.e., *ahk2-5 ahk3-7*; *ahk23*, *ahk2-5*
157 *cre1-2*; *ahk24*, *ahk3-7 cre1-2*; *ahk34*) five-day-old seedlings (Riefler et al., 2006).
158 Five days after grafting, we selected plants (scion/rootstock: WT/WT, WT/*ahk2*,
159 WT/*ahk3*, WT/*ahk4*, WT/*ahk23*, WT/*ahk24*, WT/*ahk34*) for further analysis if they
160 showed vigorous growth without adventitious roots. Grafted plants were then cultivated
161 for 7 days on either half-strength MS (1/2 MS) medium or nutrient-rich soil. We measured
162 shoot fresh weight, leaf blade area, and leaf number. Overall, WT/*ahk3*, WT/*ahk23*, and
163 WT/*ahk34* displayed greater shoot growth than WT/WT (Fig. 1A, Supplementary Fig.
164 S1A). Relative to the WT/WT control, these lines showed an increase in shoot fresh
165 weight of 26%, 35%, and 19%, and in leaf blade area of 26%, 32%, and 17%, respectively
166 (Fig. 1, B and C). Under nutrient-rich soil conditions, shoot fresh weight increased by
167 34%, 25%, and 22%, and leaf blade area by 32%, 21%, and 17% in WT/*ahk3*, WT/*ahk23*,
168 and WT/*ahk34*, respectively, compared with WT/WT (Supplementary Fig. S1, B and C).

169 Leaf number was generally similar across grafted plants in both conditions (Fig. 1D,
170 Supplementary Fig. S1D). We next monitored primary root length in grafted plants
171 transferred to 1/2 MS medium over a five-day period. Primary root length was
172 comparable at day 0, but WT/*ahk3*, WT/*ahk23*, and WT/*ahk34* developed significantly
173 shorter roots than WT/WT from day 3 onward (Supplementary Fig. S2). In contrast,
174 WT/*ahk2*, WT/*ahk4*, and WT/*ahk24* showed no significant differences in shoot or root
175 growth relative to WT/WT (Fig. 1, Supplementary Figs. S1 and S2). Notably, the relative
176 growth of WT/*ahk3* was comparable to WT/*ahk23* and WT/*ahk34*, indicating that loss of
177 AHK3 alone is sufficient to alter overall plant growth. We therefore focused subsequent
178 analyses on WT/*ahk3*, using WT/WT, WT/*ahk2*, and WT/*ahk4* as comparisons.
179

180 **Root-expressed AHK3 modulates root CK levels**

181 Our previous work showed that root-specific deficiencies of *AHK2* and *AHK3* markedly
182 increased iP- and *t*Z-type CK levels in roots, but the receptor responsible for governing
183 root CK levels was unclear (Monden et al., 2022). To clarify this, we measured iP- and
184 *t*Z-type CK concentrations in WT/WT, WT/*ahk2*, WT/*ahk3*, and WT/*ahk4* roots. Root
185 concentrations of nearly all iP- and *t*Z-type CK species were significantly elevated in
186 WT/*ahk3* compared with WT/WT (Fig. 2, Supplementary Fig. S3). In contrast, root iP-
187 and *t*Z-type CKs were largely unchanged in WT/*ahk2* and WT/*ahk4* relative to WT/WT,
188 except for iP7G and iP9G in WT/*ahk4* (Fig. 2, Supplementary Fig. S3). These findings
189 indicate that AHK3 expressed in roots modulates CK homeostasis.
190

191 **Root-expressed AHK3 influences the root transcriptome**

192 Despite the fact that *AHK2*, *AHK3*, and *AHK4* are all expressed in roots (Higuchi et al.,
193 2004), only AHK3 strongly affected root CK levels. This suggests that each CK receptor
194 may regulate a distinct set of downstream genes. To test this hypothesis, we performed
195 an RNA-seq analysis of root samples taken from WT/WT, WT/*ahk2*, WT/*ahk3*, and
196 WT/*ahk4*. All data, including raw read counts, reads per million mapped reads (RPM),
197 and normalized transcript levels are presented in Supplementary Tables S2–4. First, we
198 examined differentially expressed genes (DEGs) between the roots of the WT/WT control
199 and three grafted plants, i.e., WT/*ahk2*, WT/*ahk3*, and WT/*ahk4* (Supplementary Table
200 S6). An analysis of the DEGs with a fold change of 1.5 or greater revealed that 62 genes
201 were significantly upregulated in WT/*ahk3* relative to WT/WT roots, whereas 91 genes
202 were downregulated (Fig. 3A, Supplementary Figs. S4 and S5). Notably, relatively few
203 DEGs were detectable in the roots of WT/*ahk2* and WT/*ahk4* (Fig. 3A, Supplementary
204 Figs. S4 and S5). Next, we conducted a Gene Ontology (GO) term enrichment analysis
205 of the 62 upregulated genes and the 87 downregulated genes (excluding *AHK3*) identified
206 in WT/*ahk3* roots. This revealed that multiple hormone-related terms, such as "Cellular
207 response to hormone stimulus" and "Hormone catabolic process," were enriched in both
208 sets (Supplementary Fig. S6). To further examine the extent to which CK receptor
209 regulates CK signaling-related genes in roots, we analyzed the expression of CK-
210 inducible and -repressible genes in the roots of grafted plants; to do so we used a curated
211 gene list (Bhargava et al., 2013). We found that the expression levels of both CK-
212 inducible and -repressible genes in the roots of WT/*ahk4* were comparable to the levels
213 detected in WT/WT (Fig. 3B). In contrast, the expression of CK-inducible genes in root
214 tissue samples was significantly lower in both WT/*ahk2* and WT/*ahk3* relative to the
215 WT/WT (Fig. 3B). Moreover, CK-repressible genes were significantly increased in

216 WT/*ahk3* and showed an increasing trend in WT/*ahk2* (Fig. 3B). Notably, the magnitude
217 of these changes was more pronounced in WT/*ahk3* than in WT/*ahk2* roots, suggesting
218 that root-expressed AHK3 plays a major role in regulating root CK signaling.

219 Next, to identify candidate gene(s) that may be responsible for increased CK
220 levels in WT/*ahk3* roots, we examined whether the DEGs observed in WT/*ahk3* roots
221 included genes that are known to be involved in CK biosynthesis and inactivation. Of
222 these genes, only *CKX4*, which is involved in CK degradation, was among the genes that
223 were downregulated genes in WT/*ahk3* roots relative to the WT/WT (Fig. 3, A and C).
224 Quantitative RT-PCR (qRT-PCR) analysis confirmed that expression of *CKX4* in roots
225 was significantly decreased in WT/*ahk3* relative to WT/WT (Fig. 3D). Taken together,
226 these results suggest that root-expressed AHK3 modulates root CK levels, potentially via
227 CKX4-mediated CK degradation.

228

229 **Root-expressed AHK3 modulates *t*Z-type CKs in xylem sap**

230 CKs synthesized in roots are transported to shoots mainly via xylem pathway (Ko et al.,
231 2014; Osugi et al., 2017). Given that we observed relatively high CK levels in WT/*ahk3*
232 roots, we hypothesized that the CK levels of xylem sap may also be altered. To verify
233 this, we measured the CK concentrations of xylem sap samples from WT/WT, WT/*ahk2*,
234 WT/*ahk3*, and WT/*ahk4*. We found that *t*Z, *t*ZR, and *t*ZRPs were relatively more
235 abundant than inactive forms of *t*Z-type CK and iP-type CKs in WT/WT xylem sap
236 (Supplementary Fig. S7A). This suggests that there is preferential root-to-shoot transport
237 of *t*Z and its precursors. Notably, the concentrations of *t*Z-type CKs were significantly
238 higher in WT/*ahk3* than in WT/WT xylem sap, while the concentrations of iP-type CKs
239 remained largely unchanged (Fig. 4, Supplementary Fig. S7B). Among the major CK

240 species detected in xylem sap, the concentration of *t*Z showed a 2.22-fold increase in
241 WT/*ahk3* relative to WT/WT xylem sap (Fig. 4B). In contrast, the concentrations of *t*ZR
242 and *t*ZRPs were both slightly higher in WT/*ahk3* than in WT/WT xylem sap, showing
243 1.20-fold and 1.37-fold increases, respectively (Fig. 4B). Finally, the concentrations of
244 iP- and *t*Z-type CKs were largely unchanged in WT/*ahk2* and WT/*ahk4* relative to
245 WT/WT xylem sap, except for *t*Z and *t*ZRPs in WT/*ahk4* (Fig. 4, Supplementary Fig.
246 S7B). Overall, these results suggest that root-expressed AHK3 modulates the xylem
247 transport of *t*Z-type CKs, especially *t*Z.
248
249 **Root-expressed AHK3 systemically influences the shoot transcriptome**
250 Next, to test whether elevated *t*Z-type CK levels in WT/*ahk3* xylem sap affected shoot
251 CK levels, we measured CK concentrations in WT/WT, WT/*ahk2*, WT/*ahk3*, and
252 WT/*ahk4* shoots. Unexpectedly, *t*Z-type CK concentrations were not higher in WT/*ahk3*
253 than in WT/WT shoots, except for *t*Z9G (Supplementary Fig. S8). Similarly, almost all
254 CK species in WT/*ahk2* and WT/*ahk4* showed no marked differences compared with
255 WT/WT (Supplementary Fig. S8). We next analyzed whether root-specific CK receptor
256 deficiency may alter the shoot transcriptomes. To do so, we performed RNA-seq on
257 WT/WT, WT/*ahk2*, WT/*ahk3*, and WT/*ahk4* shoots. Raw read counts, RPM, and
258 normalized transcript levels are provided in Supplementary Tables S2, S3, and S5.
259 Differential expression analysis with a 1.5-fold cutoff revealed 163 genes significantly
260 upregulated and 35 genes downregulated in WT/*ahk3* relative to WT/WT shoots (Fig. 5A,
261 Supplementary Table S7). No DEGs were detected in WT/*ahk2* or WT/*ahk4* shoots (Fig.
262 5A, Supplementary Table S7). Moreover, the number of upregulated genes was about
263 five times greater than the number of downregulated genes in WT/*ahk3* shoots (Fig. 5A,

264 Supplementary Table S7). This finding indicates that root-specific *AHK3* deficiency
265 mainly induces gene expression in shoots.

266 To gain insight into the functional characteristics of the upregulated set, we
267 performed GO enrichment analysis using the set of 163 upregulated genes. Enriched
268 categories included "Translation," "Response to inorganic substance," and "Cellular
269 nitrogen compound biosynthetic process" (Fig. 5B), indicating activation of genes related
270 to protein synthesis, nutrient responses, and nitrogen metabolism in WT/*ahk3* shoots. We
271 then examined whether these transcriptional changes correlated with altered shoot
272 element concentrations. We found that the shoot concentrations of calcium, sulfur,
273 manganese, and molybdenum were significantly higher in WT/*ahk3* than in WT/WT
274 (Supplementary Fig. S9), suggesting a possible association between these nutrients and
275 altered gene expression in WT/*ahk3* shoots. In contrast, although several nitrogen-related
276 GO terms were enriched, shoot concentrations of nitrogen and nitrate did not differ
277 between WT/WT and WT/*ahk3* (Supplementary Fig. S9). Thus, nitrogen status in
278 WT/*ahk3* shoots did not drive the transcriptional changes observed in protein synthesis
279 and nitrogen metabolism genes. Because nitrogen is a major protein component and both
280 nitrate and CK signaling promote expressions of protein synthesis-related genes
281 (Sakakibara et al., 2006), altered CK response in WT/*ahk3* shoots may underlie these
282 transcriptional effects.

283 To further assess CK response, we compared the 163 upregulated genes in
284 WT/*ahk3* shoots with CK-inducible genes (Bhargava et al., 2013). *Arabidopsis response*
285 *regulator 5* (*ARR5*) and *Glutaredoxin-S6* (*GrxS6*) were among the overlapping genes (Fig.
286 5A). *ARR5*, one of ten type-A *ARRs*, is a representative CK-responsive gene functioning
287 as a negative feedback regulator of CK signaling (To et al., 2004). Expression of several

288 other type-A *ARRs* also tended to increase in WT/*ahk3* relative to WT/WT (Fig. 5C).
289 Consistent with the RNA-seq results, qRT-PCR confirmed that *ARR5* expression was
290 significantly higher in WT/*ahk3* shoots than in WT/WT (Fig. 5D). Taken together, these
291 results indicate that root-expressed AHK3 modulates shoot gene expression, at least
292 partly through activation of CK signaling.
293
294 **Root-derived CK signals are required for enhanced shoot growth via root-expressed**
295 **AHK3**
296 Elevated *t*Z-type CKs in WT/*ahk3* xylem sap suggested that long-distance signals of root-
297 derived *t*Z-type CK contribute to enhanced shoot growth. To test this, we generated *ahk3*
298 *abcg14* and *ahk3 cyp735a1 cyp735a2* (*ahk3 cypDM*) mutants by traditional crossing
299 (Supplementary Fig. S10A). Since both *abcg14* and *cypDM* shoots display lack proper
300 root-derived *t*Z-type CK signaling (Kiba et al., 2013; Ko et al., 2014), these mutants allow
301 assessment of its contribution. Disruption of the respective genes in *ahk3 abcg14* and
302 *ahk3 cypDM* was confirmed by RT-PCR (Supplementary Fig. S10B). Grafted plants
303 (scion/rootstock: WT/WT, WT/*ahk3*, WT/*abcg14*, WT/*ahk3 abcg14*, WT/*cypDM*,
304 WT/*ahk3 cypDM*) were cultivated on 1/2 MS medium, and shoot growth was measured.
305 Shoot fresh weight and leaf blade area were significantly reduced in WT/*abcg14* and
306 WT/*ahk3 abcg14*, while WT/*cypDM* and WT/*ahk3 cypDM* showed no decrease
307 compared with WT/WT (Fig. 6, A and B). These results agree with previous findings that
308 root-specific deficiency of *ABCG14* impairs shoot growth, whereas deficiencies of
309 *CYP735A1* and *CYP735A2* do not (Kiba et al., 2013; Ko et al., 2014). Notably, the
310 increases in shoot fresh weight and leaf blade area seen in WT/*ahk3* compared with
311 WT/WT were largely suppressed by disrupting *ABCG14* and completely abolished by

312 disrupting *CYP735A1* and *CYP735A2* in roots (Fig. 6, A and B). These findings indicate
313 that long-distance signals of root-derived *t*Z-type CKs are required for enhanced shoot
314 growth in WT/*ahk3*.

315 To determine which shoot-expressed CK receptor(s) mediate CK signaling
316 underlying this growth effect, we analyzed grafted plants carrying single or double
317 mutations in *AHK2*, *AHK3*, or *AHK4* specifically in WT/*ahk3* shoots. Grafted plants
318 (scion/rootstock: WT/WT, WT/*ahk3*, *ahk2*/*ahk3*, *ahk3*/*ahk3*, *ahk4*/*ahk3*, *ahk23*/*ahk3*,
319 *ahk24*/*ahk3*, *ahk34*/*ahk3*) were cultivated under 1/2 MS medium, and shoot growth was
320 measured. Increases in shoot fresh weight and leaf blade area observed in WT/*ahk3*
321 relative to WT/WT were similarly evident in *ahk2*/*ahk3*, *ahk4*/*ahk3*, and *ahk24*/*ahk3* (Fig.
322 6, C and D). In contrast, these enhancements were suppressed in *ahk3*/*ahk3* and
323 *ahk34*/*ahk3*, and markedly reduced in *ahk23*/*ahk3*, where values were significantly lower
324 than WT/WT (Fig. 6, C and D). These results indicate that enhanced shoot growth in
325 WT/*ahk3* depends primarily on CK signaling through shoot-expressed AHK3, with
326 partial contribution from AHK2. Next, to visualize sites of enhanced CK response in
327 WT/*ahk3* shoots, we introduced the synthetic CK reporter *TCSn:GFP* into WT/WT and
328 WT/*ahk3* shoots (Zürcher et al., 2013). Grafted plants (scion/rootstock: *TCSn:GFP*/WT,
329 *TCSn:GFP*/*ahk3*) were grown on 1/2 MS medium. *TCSn:GFP*/*ahk3* exhibited greater
330 shoot fresh weight and leaf blade area than *TCSn:GFP*/WT (Fig. 6E). Notably, GFP
331 fluorescence intensity in true leaf was also significantly higher in *TCSn:GFP*/*ahk3* than
332 in *TCSn:GFP*/WT (Fig. 6F). Finally, to examine how root-specific *AHK3* deficiency
333 influences leaf micro-morphology, we measured epidermal cell size and number in true
334 leaves of WT/WT and WT/*ahk3*. Cell size was comparable between genotypes, but cell
335 number was significantly higher in WT/*ahk3* than in WT/WT (Fig. 6G). These results

336 suggest that root-specific *AHK3* deficiency enhances leaf CK response, promoting
337 epidermal cell division and thereby increasing leaf size.
338
339 **Root-expressed AHK3 modulates leaf size in a nitrate-dependent manner**
340 *AHK3* was identified as one of the top genes co-expressed with the nitrate sensor NLP7
341 (Supplementary Table S1), suggesting that AHK3 may play a role in plant nitrate
342 responses. To test this, we manipulated the nitrate levels of WT/WT and WT/*ahk3* roots.
343 Ten-day-old WT/WT and WT/*ahk3* were first transferred to 2.5 mM ammonium
344 succinate (5 mM NH_4^+) medium and incubated for 48 hours to deplete nitrate
345 (Supplementary Fig. S11A). Grafted plants were then transferred to medium containing
346 5 mM NH_4^+ supplemented with either 0.5 mM KNO_3 (KNO_3) or 0.5 mM KCl (KCl) and
347 grown for 5 days to assess the presence or absence of nitrate signaling in roots. Nitrate
348 accumulated only in WT/WT and WT/*ahk3* roots grown under KNO_3 (Supplementary
349 Fig. S11B). Moreover, WT/WT and WT/*ahk3* appeared healthy, with comparable shoot
350 chlorophyll concentrations under both conditions (Supplementary Fig. S12), indicating
351 that nitrogen deficiency or ammonium toxicity did not occur. In WT/WT, shoot fresh
352 weight and leaf blade area were found to be significantly greater under KNO_3 than KCl
353 (Fig. 7A), showing that nitrate signaling promotes leaf growth. Notably, shoot fresh
354 weight and leaf blade area were similar between WT/WT and WT/*ahk3* under KCl, but
355 were higher in WT/*ahk3* than in WT/WT under KNO_3 (Fig. 7A).
356 Next, to test whether nitrate-dependent growth promotion in WT/*ahk3*
357 requires root-derived *t*Z-type CK signals, we analyzed WT/*abcg14* and WT/*ahk3 abcg14*
358 grown under KNO_3 or KCl. Interestingly, the increases in shoot fresh weight and leaf
359 blade area observed in WT/WT and WT/*ahk3* under KNO_3 were strongly suppressed in

360 WT/*abcg14* and WT/*ahk3 abcg14* (Fig. 7B). These results indicate that long-distance
361 signals of root-derived *t*Z-type CKs are required for nitrate-induced leaf growth
362 promotion. Moreover, shoot fresh weight and leaf blade area were comparable between
363 WT/*abcg14* and WT/*ahk3 abcg14* under KNO_3 (Fig. 7B), suggesting that root-derived
364 *t*Z-type CK signals may contribute to the enhanced leaf growth of WT/*ahk3*.

365 To further clarify the role of AHK3 in nitrate signaling, we analyzed
366 expression of CK biosynthesis and inactivation genes in roots 4 hours after transfer to
367 KNO_3 or KCl. Nitrate accumulation was detected only in WT/WT and WT/*ahk3* roots
368 after KNO_3 treatment (Supplementary Fig. S11C). In WT/WT, root expression of *IPT3*,
369 *CYP735A1*, *CYP735A2*, and *CKX4* was significantly higher under KNO_3 than KCl (Fig.
370 7C, Supplementary Fig. S13), indicating induction by nitrate signaling. Importantly,
371 expression of *IPT3*, *CYP735A1*, and *CYP735A2* was similar in WT/WT and WT/*ahk3*
372 under KNO_3, whereas *CKX4* expression was significantly reduced in WT/*ahk3* compared
373 with WT/WT (Fig. 7C, Supplementary Fig. S13). These results suggest that both nitrate
374 signals and root-expressed AHK3 are required for maximal *CKX4* induction.

375 To investigate the role of CKX4 in nitrate signaling, we obtained two
376 independent T-DNA alleles, *ckx4-1* (SALK_055204) and *ckx4-2* (SALK_132516), from
377 the Arabidopsis Biological Resource Center. *Ckx4-1* carries an intron insertion (Bartrina
378 et al., 2011), while *ckx4-2* carries an exon insertion (Supplementary Fig. S14). RT-PCR
379 confirmed reduced *CKX4* transcript in *ckx4-1* and absence in *ckx4-2* (Fig. 7D), indicating
380 that *ckx4-1* is a knockdown and *ckx4-2* a knockout. Grafted plants (scion/rootstock:
381 WT/WT, WT/*ckx4-1*, WT/*ckx4-2*) were cultivated under KNO_3 or KCl, and shoot growth
382 was measured. Under KCl, shoot fresh weight and leaf blade area were similar among

383 genotypes (Fig. 7E). Under KNO_3, however, both traits were significantly greater in
384 WT/*ckx4-1* and WT/*ckx4-2* compared to WT/WT (Fig. 7E).

385 To further clarify relationship between AHK3 and CKX4, we generated *ahk3*
386 *ckx4-1* and *ahk3 ckx4-2* mutants by traditional crossing (Supplementary Fig. S15, A and
387 B). Grafted plants (scion/rootstock: WT/WT, WT/*ahk3*, WT/*ckx4-1*, WT/*ckx4-2*,
388 WT/*ahk3 ckx4-1*, WT/*ahk3 ckx4-2*) were grown under KNO_3 or KCl, and shoot growth
389 was measured. All genotypes showed comparable shoot growth under KCl
390 (Supplementary Fig. S15C). Under KNO_3, however, shoot fresh weight and leaf blade
391 area were significantly greater in WT/*ahk3*, WT/*ckx4-1*, WT/*ckx4-2*, WT/*ahk3 ckx4-1*,
392 and WT/*ahk3 ckx4-2* compared with WT/WT (Supplementary Fig. S15C). These traits
393 were significantly higher in WT/*ahk3* than in WT/*ckx4-1* and WT/*ckx4-2* (Supplementary
394 Fig. S15C), indicating that CKX4 acts downstream of AHK3. Importantly, WT/*ahk3*
395 *ckx4-1* and WT/*ahk3 ckx4-2* showed no further growth increase relative to WT/*ahk3*
396 under KNO_3 (Supplementary Fig. S15C). Together, these results suggest that nitrate-
397 induced leaf growth promotion occurs through a pathway mediated jointly by AHK3 and
398 CKX4.

399

400 **DISCUSSION**

401 Recent studies have shown that long-distance signals of root-derived *t*Z-type CK
402 coordinate multiple physiological processes in aerial organs, including leaf growth,
403 photoperiod stress response, shade avoidance, and flowering time (Osugi et al., 2017;
404 Landrein et al., 2018; Frank et al., 2020; Gautrat et al., 2024; Bartrina et al., 2025). These
405 findings highlight that proper modulation of root-to-shoot *t*Z-type CK transport is
406 essential for plants to adapt to environmental fluctuations.

407 Based on our findings and prior studies (Miyawaki et al., 2004; Kiba et al.,
408 2013; Ko et al., 2014; Zhang et al., 2014; Sakakibara, 2021, 2025), we provide new
409 insight into the specific mechanisms responsible for modulating xylem *t*Z-type CK
410 transport, as mediated by CK perception and degradation through an AHK3–CKX4
411 module. Nitrate signaling promotes *t*Z-type CK biosynthesis in pericycle and phloem
412 companion cells via IPT3, CYP735A2, and related enzymes. *t*Z-type CKs are then
413 transported to the extracellular and endoplasmic reticulum (ER) space by transporters
414 such as ABCG14. Active form *t*Z are perceived by AHK3 on plasma membrane (PM)
415 and ER membrane. Activation of CK signaling through AHK3 induces expression of
416 *CKX4*, predicted to localize in apoplast, where it reduces apoplastic *t*Z-type CK levels by
417 degradation. These mechanisms likely influence the apoplastic *t*Z-type CK pool and,
418 consequently, the amount of *t*Z-type CK loaded into xylem (Supplementary Fig. S16). To
419 further substantiate this model, it will likely be necessary to analyze the spatial expression
420 patterns of AHK3 and CKX4 at the tissue and cellular level in future studies. Interestingly,
421 *IPT3* expression and *t*Z-type CK levels in roots also respond to other nutrients, including
422 phosphate, sulfate, and potassium (Hirose et al., 2008; Nam et al., 2012). Thus, AHK3
423 may modulates *t*Z-type CK levels in response to diverse nutrient signals. Collectively,
424 the AHK3–CKX4 module could serve as a feedback regulator that attenuates the nutrient-
425 induced xylem transport of *t*Z-type CKs, thereby fine-tuning leaf CK response to maintain
426 balanced plant growth.

427 Root-specific deficiency of *AHK3* enhanced shoot growth but decreased
428 primary root growth, resulting in an imbalance in whole-plant growth (Fig. 1,
429 Supplementary Fig. S2). Given that primary root length in *ahk3* is comparable to that in
430 Col-0 (Riefler et al., 2006), the reduced root growth observed in WT/*ahk3* is considered

431 a compensatory response to enhanced shoot growth. Interestingly, a temporal analysis of
432 shoot growth in grafted plants revealed that WT/*ahk3* exhibited a significant increase in
433 leaf blade area 3 days after transfer to 1/2 MS medium, which coincided with the onset
434 of primary root growth inhibition (Supplementary Figs. S2 and S17). Furthermore, not
435 only was shoot growth enhancement attenuated in *ahk3*/*ahk3*, but primary root growth
436 inhibition was also diminished (Fig. 6, Supplementary Fig. S17), suggesting that shoot
437 and root growth may change in a correlated manner. Taken together, these results indicate
438 that root-expressed AHK3 is physiologically important for maintaining whole-plant
439 growth balance by modulating xylem *t*Z-type CK transport and leaf CK status, thereby
440 preventing excessive energy investment in shoot growth and coordinating energy
441 allocation between shoots and roots.

442 CKXs are known to mediate irreversible CK degradation, producing adenine
443 (or its derivatives) and aldehyde (Schmülling et al., 2003). In *Arabidopsis*, seven CKXs
444 differ in substrate specificity, spatial and temporal expression, and subcellular
445 localization, targeting either vacuoles (CKX1, CKX3), ER (CKX1), apoplasts (CKX2,
446 CKX4, CKX5, CKX6), or the cytosol (CKX7) (Werner et al., 2003; Galuszka et al., 2007;
447 Frébort et al., 2011; Niemann et al., 2018). Expression of *CKX3*, *CKX4*, *CKX5*, and *CKX6*
448 is strongly induced by CK treatment (Werner et al., 2006), suggesting sensitivity to
449 internal CK levels and roles in maintaining homeostasis. Moreover, CKX2 and CKX4
450 show higher *in vitro* CKX activity than other CKXs, preferentially degrading active form
451 CKs at neutral or slightly basic pH (Galuszka et al., 2007). Our data showed that root-
452 specific *AHK3* deficiency greatly reduced *CKX4* expression in roots, without significantly
453 altering other *CKX*s (Figs. 3 and 7). These findings suggest that root-expressed AHK3
454 modulates *t*Z degradation by inducing *CKX4* expression in response to the internal *t*Z

455 level. This interpretation is supported by our observation that *t*Z concentration was
456 markedly higher in WT/*ahk3* xylem sap than in WT/WT (Fig. 4). Furthermore, Osugi *et*
457 *al.* (2017) demonstrated that root-derived *t*ZR controls both leaf number and area,
458 whereas root-derived *t*Z regulates only leaf area. In WT/*ahk3*, the increase in xylem sap
459 *t*Z relative to WT/WT was greater than that of *t*ZR (Fig. 4). Thus, the enlarged leaf blade
460 area in WT/*ahk3*, without a change in leaf number, likely reflects long-distance signaling
461 by root-derived *t*Z (Figs. 1 and 4).

462 AHK2, AHK3, and AHK4 localize to the PM and ER membrane, where they
463 play central roles in CK signal transduction (Antoniadi et al., 2020; Kubiasová et al.,
464 2020). AHK3 is considered to be primarily localized on the ER membrane and partially
465 on the PM (Caesar et al., 2011; Wulfetange et al., 2011). Therefore, ER-localized AHK3
466 may contribute substantially to modulation of xylem transport of *t*Z-type CKs. AHK3 is
467 also expressed more strongly in leaves than in roots, and its leaf expression exceeds that
468 of AHK2 and AHK4, supporting its hypothesized role as a major regulator of leaf CK
469 response (Higuchi et al., 2004). This hypothesis is consistent with our finding that leaf
470 growth promotion, driven by increased shoot CK response, was diminished when AHK3
471 was specifically disrupted in WT/*ahk3* shoots (Fig. 6). Strikingly, root-expressed AHK3
472 exerted a stronger impact on the root transcriptome and on CK levels than root-expressed
473 AHK2 and AHK4 (Figs. 2 and 3). Taken together, these results suggest that AHK3 also
474 plays a major role in roots. Previous reports indicate that rosette leaf growth, CK
475 metabolism, leaf senescence, stomatal opening, and embryo growth depend particularly
476 on AHK3, as disruption of AHK3, but not other CK receptors, impairs these processes
477 (Riefler et al., 2006; Kim et al., 2006; Arnaud et al., 2017; Loperfido et al., 2025). The
478 distinct functions of these receptors may arise from their expression patterns, recognition

479 of different CK species, and specific interactions with other proteins (Higuchi et al., 2004;
480 Spíchal et al., 2004; Romanov et al., 2006; Stolz et al., 2011). A key feature of AHK3 is
481 its ligand preference: while AHK2 and AHK4 bind iP and *t*Z with similar affinity, AHK3
482 shows higher affinity for *t*Z than iP (Stolz et al., 2011). In addition, AHK3 specifically
483 mediates CK-triggered phosphorylation of ARR2 (Kim et al., 2006). These differences in
484 ligand preference and downstream targets may underlie the unique functions of AHK3.
485 Overall, this study uncovered a comprehensive mechanism by which the CK
486 receptor AHK3 systemically modulates the shoot growth via exerting control of xylem
487 *t*Z-type CK transport. Furthermore, we clarified the role of AHK3 in modulating leaf size
488 in response to root nitrogen availability, a key environmental factor. Overall, these
489 findings provide new insight into how plants integrate nutritional cues to coordinate
490 systemic communication between roots and shoots.
491

492 **MATERIALS AND METHODS**

493 **Plant materials**

494 The *Arabidopsis thaliana* accession Col-0 was used as wild type. T-DNA insertion lines
495 *ahk2-5*, *ahk3-7*, *cre1-2*, *ahk2-5 ahk3-7*, *ahk2-5 cre1-2*, *ahk3-7 cre1-2* (Riefler et al., 2006),
496 *abcg14* (Ko et al., 2014), *cyp735a1-2 cyp735a2-2* (Kiba et al., 2013), and *ckx4-1*
497 (Bartrina et al., 2011) have been described previously. The *ckx4-2* (SALK_132516) line
498 was obtained from the Arabidopsis Biological Resource Center (https://abrc.osu.edu/).
499 The transgenic line *TCSn:GFP* (Zürcher et al., 2013) was described previously. Finally,
500 the homozygous multiple mutants *ahk3-7 abcg14*, *ahk3-7 cyp735a1-2 cyp735a2-2*, *ahk3-*
501 *7 ckx4-1*, and *ahk3-7 ckx4-2* were generated by crossing, and genotypes were determined
502 by genomic PCR using primers listed in Supplementary Table S8.

503

504 **Growth conditions of grafted plants**

505 Seeds were surface-sterilized and kept in the dark at 4°C for 3 days to break dormancy.
506 Approximately 120 seeds per dish were sown in rectangular dishes (140 × 100 × 20 mm^3;
507 Eiken Chemical Co. Ltd., Tokyo, Japan) containing 50 mL of half-strength MS salts
508 including vitamins (Code: M0222; Duchefa Biochemie), supplemented with 0.05% (w/v)
509 MES-KOH (pH 5.7), 1% (w/v) sucrose, and 0.5% (w/v) gellan gum (Fujifilm Wako, VA,
510 USA). Plants were grown under a 16/8-h light/dark cycle at 22°C with a photosynthetic
511 photon flux density (PPFD) of 25 μmol m^{-2} s^{-1}. Five-day-old seedlings were cut
512 perpendicularly at the hypocotyl using an injection needle tip (Code: NN-2613S;
513 TERUMO, Tokyo, Japan). Excised scions were connected to corresponding rootstocks
514 using silicone microtubes (inner × outer diameter: φ0.4 × φ0.5 mm; Code: 1-8194-04; AS
515 ONE, Osaka, Japan). Grafted plants were incubated for 5 days under continuous light at
516 27°C with a PPFD of 50 μmol m^{-2} s^{-1}. Successfully grafted plants without adventitious
517 roots were selected, transferred to solid media or soil pots, then grown for further
518 experiments.

519 For *in vitro* cultures, grafted plants were grown vertically for five days or
520 horizontally for seven days under a PPFD of 70 μmol m^{-2} s^{-1} (16/8-h light/dark cycle) at
521 22°C in 50 mL (vertical) or 30 mL (horizontal) of half-strength MS salts without vitamins
522 (Code: M0221; Duchefa Biochemie), supplemented with 0.05% (w/v) MES-KOH (pH
523 5.7), 1% (w/v) sucrose, and 0.8% (w/v) purified agar (Code: 01162-15; Nacalai Tesque,
524 Kyoto, Japan). To facilitate non-destructive root sampling during horizontal growth,
525 media surfaces were covered with cellophane sheets (Hachiya et al., 2021).

526 For soil cultivation, grafted plants were grown for 7 days under a PPFD of
527 70 μmol m^{-2} s^{-1} (16/8-h light/dark cycle) at 22°C in pots containing ~150 mL of nutrient-
528 rich soil (Supermix A; Sakata Seed, Kyoto, Japan).
529 For transfer experiments with varying nitrogen concentrations, grafted plants
530 were placed on cellophane sheets in round dishes (diameter 90 mm; depth 20 mm; AS
531 ONE) containing 30 mL of half-strength MS modified basal salt mixture without nitrogen
532 (M531; PhytoTech Labs, Lenexa, KS, USA), supplemented with 2.5 mM $(NH_4)_2C_4H_4O_4$,
533 0.05% (w/v) MES-KOH (pH 5.7), 1% (w/v) sucrose, and 0.8% (w/v) purified agar (Code:
534 01162-15; Nacalai Tesque) (5 mM NH_4^+ medium). Plants were grown for 48 hours under
535 a PPFD of 70 μmol m^{-2} s^{-1} (16/8-h light/dark cycle) at 22°C, then transferred to 5 mM
536 NH_4^+ medium supplemented with either 0.5 mM KNO_3 or 0.5 mM KCl and grown for
537 five days under the same conditions.
538
539 **Growth analysis of grafted plants**
540 Shoots were weighed on a precision balance (HR-202i; A&D, Tokyo, Japan). All leaf
541 blades were harvested and scanned at 600 dpi (GT-X980; EPSON, Tokyo, Japan) to
542 measure true leaf blade area. Roots of vertically grown plants were scanned at 600 dpi to
543 measure primary root length. To monitor root elongation, root tip positions were marked
544 every 24 hours. Leaf blade area and primary root length were quantified using ImageJ
545 version 1.53t (US National Institutes of Health, Bethesda, MD, USA).
546
547 **Xylem sap collection**
548 Grafted plants were cut perpendicularly at the hypocotyl using an injection needle tip
549 (Code: NN-2613S; TERUMO). A silicone microtube (inner × outer diameter: φ0.5 × φ0.6

550 mm; Code: 1-8194-05; AS ONE) was attached to the cut end, and plants were incubated
551 for 2 hours to allow exudation. After incubation, the silicone microtube was detached,
552 and xylem sap collected in the tube was recovered by centrifugation into a collection tube.
553 This was then and stored at –80°C until further analysis. We used 12 µL aliquots of sap
554 from each grafted plant for CK analyses.
555
556 **Determination of CK species**
557 CK extraction and quantification followed the method of Kojima *et al*. (2009), using an
558 ultra-performance liquid chromatography–tandem quadrupole mass spectrometry system
559 (AQUITY UPLC System/XEVO-TQS; Waters Corp., Milford, MA, USA) equipped with
560 an octadecylsilyl column (ACQUITY UPLC HSS T3, 1.8 µm, 2.1 mm × 100 mm; Waters
561 Corp.).
562
563 **Extraction of total RNA**
564 To extract total RNA, frozen plant samples were first homogenized using a Multi-Beads
565 Shocker and 5 mm zirconia beads. Total RNA was then isolated with the RNeasy Plant
566 Mini Kit (Qiagen, Hilden, Germany) with all protocols performed as per the
567 manufacturer's protocol. For RNA-seq library preparation, RNA was further purified by
568 on-column DNase digestion (Qiagen).
569
570 **RNA-seq analysis**
571 RNA quality was evaluated using a Qubit RNA IQ Assay Kit with a Qubit 4 Fluorometer
572 (Thermo Fisher Scientific, Tokyo, Japan). Samples with RNA IQ scores of 9.5–10.0 were
573 used for RNA-seq. cDNA libraries were prepared with the NEBNext Ultra II Directional

574 RNA Library Prep Kit (E7760S, New England Biolabs, Ipswich, MA, USA), SPRIselect
575 (B23317, Beckman Coulter), the NEBNext Poly(A) mRNA Magnetic Isolation Module
576 (E7490S, New England Biolabs), and NEBNext Multiplex Oligos for Illumina (E7710S,
577 New England Biolabs), with all steps following the manufacturer's instructions. Libraries
578 were sequenced on a NextSeq 500 (Illumina, San Diego, CA, USA), and bcl files were
579 converted to fastq using bcl2fastq (Illumina). Reads were analyzed as described by
580 Notaguchi *et al*. (2014) and mapped to the *Arabidopsis* reference (TAIR10) using Bowtie
581 (Langmead et al., 2009) with the options "--all --best --strata." For normalization, read
582 count data were transformed with rlog and adjusted by subtracting the average expression
583 for each gene using default settings of iDEP v0.96 (Ge et al., 2018). DEGs were extracted
584 using edgeR with a false discovery rate cutoff of 0.15 under the default settings of
585 RNAseqChef v1.1.4 (Etoh et al., 2023). Gene set enrichment was performed using
586 ShinyGO v0.82 (Ge et al., 2020) using the default parameters. During analysis we focused
587 on the Biological Process annotation category.
588
589 **Reverse transcription and quantitative RT-PCR**
590 Reverse transcription was performed with the ReverTraAce qPCR RT Master Mix with
591 gDNA Remover (Toyobo, Osaka, Japan). For each reaction, 0.5 µg of RNA was used as
592 input. Synthesized cDNA was diluted five-fold with sterile water and used as template
593 for qRT-PCR. Reactions were run on a QuantStudio 1 system (Thermo Fisher Scientific)
594 using a KOD SYBR qPCR Mix (Toyobo). Relative expression was determined using the
595 comparative Ct method. *TIP41* was used as an internal reference gene. Primer sequences
596 are listed in Supplementary Table S9.
597

598 **Determination of nutrient elements**

599 Shoots were harvested and oven-dried at 80°C for 2 days, ground with a spoon, then
600 stored in a desiccator with silica gel. For carbon and nitrogen quantification, we weighed
601 portions of dried samples, packed them into tin capsules, and subjected them to
602 quantitative analysis using a vario MICRO cube elemental analyzer (Elementar
603 Analysensysteme GmbH, Hanau, Germany). For other elements (e.g., potassium, calcium,
604 sulfur, phosphorus, magnesium, sodium, manganese, zinc, iron, boron, copper,
605 molybdenum, and cobalt), weighed portions of dried samples were digested with HNO_3
606 followed by H_2O_2. Digests were suspended in 1 mL of 0.08 M HNO_3, diluted tenfold with
607 0.08 M HNO_3, and analyzed using inductively coupled plasma mass spectrometry
608 (Agilent 7800 ICP-MS; Agilent Technologies, Santa Clara, CA, USA). Here, indium was
609 used as an internal standard.

610

611 **Nitrate level determination**

612 Nitrate was extracted using 10 volumes of sterile water at 100°C for 20 min. A 5.0 μL
613 aliquot of supernatant was mixed with 40 μL of 5% (w/v) salicylic acid in concentrated
614 sulfuric acid and incubated at room temperature for 20 min. A mock treatment with 40
615 μL concentrated sulfuric acid was prepared in parallel. Finally, 1 mL of 8% (w/v) NaOH
616 was added to the mixture, and nitrate concentrations was determined by recording sample
617 absorbance at 410 nm.

618

619 **Fluorescence microscopy**

620 Fluorescence imaging was performed using an all-in-one fluorescence microscope (BZ-
621 X710, KEYENCE, Osaka, Japan) equipped with a 4× objective (CFI Plan Fluor DL

622 4×/0.13, Nikon, Tokyo, Japan) and a metal halide lamp (No. 91056, KEYENCE). A
623 narrow-band GFP filter (Ex. 480/20; Em. 510/20; 49020, Chroma, Brattleboro, VT, USA)
624 was used for GFP detection, and a Cy5 filter (Ex. 620/60; Em. 700/75; 49006, Chroma)
625 was used for chlorophyll autofluorescence. All images were acquired using identical
626 exposure times. For quantification of GFP fluorescence, background signals were
627 subtracted by using non-fluorescent regions as reference.
628
629 **Leaf cellular analysis**
630 The fifth true leaf was excised from the shoot and scanned at 600 dpi (GT-X980; EPSON)
631 to measure total leaf area. The abaxial surface was pressed onto Scotch transparent
632 adhesive tape (Code: 500-3-15-10P; 3M Japan, Tokyo, Japan) and carefully peeled to
633 isolate epidermal cells. Epidermal cell images were captured using a fluorescence
634 microscope (BZ-X710; KEYENCE) equipped with a 20× objective (CFI Plan Apo
635 20×/0.75; Nikon). Thirty epidermal cells were randomly selected, and their areas were
636 measured using ImageJ v1.53t (US National Institutes of Health, Bethesda). The mean
637 area of 30 cells was defined as epidermal cell size. The total epidermal cell number was
638 estimated by dividing the total leaf area by the mean cell size.
639
640 **Statistical analyses**
641 Data were analyzed using unpaired two-tailed Welch's *t*-tests and Tukey–Kramer
642 multiple comparison test. All statistical analyses were conducted in R v4.3.0 (R
643 Foundation for Statistical Computing, Vienna, Austria).
644
645 **AUTHOR CONTRIBUTIONS**

K.M. and T.H. conceived and designed experiments. K.M., T.S., M.K., Y.T., T.Ka., H.S., and T.H. performed the experiments and data analysis. T.Ki., T.N., and T.H. supervised the study. K.M. wrote the manuscript with contributions from all authors. All authors approved the final manuscript.

ACKNOWLEDGEMENTS

We thank Dr. Ryo Tabata and Dr. Tomoko Niwa for technical advice, Ms. Maki Saiki for ICP-MS analysis, and Prof. Thomas Schmülling for important input. We also acknowledge the use of ChatGPT, an AI-based language tool, for support in clarifying the manuscript, and Enago (www.enago.jp) for English language review. This study was supported by grants from JSPS KAKENHI [No. JP24KJ1709 to K.M., No. 21H02087 to T.Ka., and Nos. 20K05771 and 23K04978 to T.H.] and from JST SPRING [No. JPMJSP2155 to K.M.].

CONFLICT OF INTEREST

The authors declare that they have no competing interests.

DATA AVAILABILITY STATEMENT

RNA-seq raw data are deposited in ArrayExpress under accession number E-MTAB-15416.

SUPPORTING INFORMATION

Additional Supporting Information is found in the online version of this article.

Figure S1. Effects of root-specific CK receptor deficiency on shoot growth in soil.

670 **Figure S2.** Effects of root-specific CK receptor deficiency on primary root length.

671 **Figure S3.** Effects of root-specific CK receptor deficiency on root concentration of
672 individual CK species.

673 **Figure S4.** Differentially expressed genes in grafted plants visualized by volcano plot.

674 **Figure S5.** Differentially expressed genes in grafted plants visualized by Venn diagram.

675 **Figure S6.** Differentially expressed genes in grafted plants visualized by gene ontology
676 terms.

677 **Figure S7.** Effects of root-specific CK receptor deficiency on xylem sap concentration
678 of individual CK species.

679 **Figure S8.** Effects of root-specific CK receptor deficiency on shoot concentration of
680 individual CK species.

681 **Figure S9.** Effects of root-specific CK receptor deficiency on shoot element
682 concentrations.

683 **Figure S10.** Genomic PCR and RT-PCR results for *ahk3 abcg14* and *ahk3 cypDM*.

684 **Figure S11.** Effects of root-specific *AHK3* deficiency on root nitrate concentration in
685 response to nitrate signaling.

686 **Figure S12.** Effects of root-specific *AHK3* deficiency on shoot chlorophyll concentration
687 in response to nitrate signaling.

688 **Figure S13.** Effects of root-specific *AHK3* deficiency on root gene expressions in
689 response to nitrate signaling.

690 **Figure S14.** Characterization of *CKX4* T-DNA insertion alleles.

691 **Figure S15.** Effects of root-specific deficiencies of *AHK3* and *CKX4* on shoot growth in
692 response to nitrate signaling.

693 **Figure S16.** A proposed model for xylem *t*Z-type CK transport controlled by AHK3 in
694 response to nitrate signaling.
695 **Figure S17.** Effects of root-specific *AHK3* deficiency on shoot and root growth.
696 **Table S1.** A list coexpressed with *NLP7* by ATTED II.
697 **Table S2.** Information about raw read counts.
698 **Table S3.** Information about reads per million mapped reads.
699 **Table S4.** Information about root normalized transcript levels.
700 **Table S5.** Information about shoot normalized transcript levels.
701 **Table S6.** Information about root DEGs.
702 **Table S7.** Information about shoot DEGs.
703 **Table S8.** Primers used in this study for genomic PCR and RT-PCR.
704 **Table S9.** Primers used in this study for qRT-PCR.
705
706 **REFERENCES**
707 Abualia, R., Ötvös, K., Novák, O., Bouguyon, E., Domanegg, K., Krapp, A. *et al*. (2022)
708 Molecular framework integrating nitrate sensing in root and auxin-guided shoot adaptive
709 responses. *Proc Natl Acad Sci U S A,* **119**(31), e2122460119.
710
711 Antoniadi, I., Novák, O., Gelová, Z., Johnson, A., Plíhal, O., Simerský, R. *et al*. (2020)
712 Cell-surface receptors enable perception of extracellular cytokinins. *Nat Commun,* **11**(1),
713 4284.
714

715 Arnaud, D., Lee, S., Takebayashi, Y., Choi, D., Choi, J., Sakakibara, H. *et al*. (2017)
716 Cytokinin-mediated regulation of reactive oxygen species homeostasis modulates
717 stomatal immunity in Arabidopsis. *Plant Cell*, **29**(3), 543–559.
718
719 Bartrina, I., Otto, E., Strnad, M., Werner, T. & Schmülling, T. (2011) Cytokinin regulates
720 the activity of reproductive meristems, flower organ size, ovule formation, and thus seed
721 yield in Arabidopsis thaliana. *Plant Cell*, **23**(1), 69–80.
722
723 Bartrina, I., Werner, S., Schenke, A., Gasperini, D., Werner, T. & Schmülling, T. (2025)
724 Root-derived cytokinin regulates Arabidopsis flowering time through components of the
725 age pathway. *Plant Physiol.*, **198**(3).
726
727 Bhargava, A., Clabaugh, I., To, J.P., Maxwell, B.B., Chiang, Y.H., Schaller, G.E. *et al*.
728 (2013) Identification of cytokinin-responsive genes using microarray meta-analysis and
729 RNA-Seq in Arabidopsis. *Plant Physiol.*, **162**(1), 272–294.
730
731 Caesar, K., Thamm, A.M.K., Witthöft, J., Elgass, K., Huppenberger, P., Grefen, C. *et al*.
732 (2011) Evidence for the localization of the Arabidopsis cytokinin receptors AHK3 and
733 AHK4 in the endoplasmic reticulum. *J. Exp. Bot.*, **62**(15), 5571–5580.
734
735 Etoh, K. & Nakao, M. (2023) A web-based integrative transcriptome analysis,
736 RNAseqChef, uncovers the cell/tissue type-dependent action of sulforaphane. *J. Biol.*
737 *Chem.*, **299**(6), 104810.
738

739 Frank, M., Cortleven, A., Novák, O. & Schmülling, T. (2020) Root-derived trans-zeatin
740 cytokinin protects Arabidopsis plants against photoperiod stress. *Plant Cell Environ.*, **43**,
741 2637–2649.
742
743 Frébort, I., Kowalska, M., Hluska, T., Frébortová, J. & Galuszka, P. (2011) Evolution of
744 cytokinin biosynthesis and degradation. *J. Exp. Bot.*, **62**(8), 2431–2452.
745
746 Galuszka, P., Popelková, H., Werner, T., Frébortová, J., Pospíšilová, H., Mik, V. *et al.*
747 (2007) Biochemical characterization of cytokinin oxidases/dehydrogenases from
748 Arabidopsis thaliana expressed in Nicotiana tabacum L. *J. Plant Growth Regul.*, **26**(3),
749 255–267.
750
751 Gautrat, P., Buti, S., Romanowski, A., Lammers, M., Matton, S.E.A., Buijs, G. *et al.*
752 (2024) Phytochrome-dependent responsiveness to root-derived cytokinins enables
753 coordinated elongation responses to combined light and nitrate cues. *Nat. Commun.*, **15**,
754 8489.
755
756 Ge, S.X., Son, E.W. & Yao, R. (2018) iDEP: an integrated web application for differential
757 expression and pathway analysis of RNA-Seq data. *BMC Bioinformatics*, **19**, 534.
758
759 Ge, S.X., Jung, D. & Yao, R. (2020) ShinyGO: a graphical gene-set enrichment tool for
760 animals and plants. Bioinformatics, **36**(8), 2628–2629.
761

762 Hachiya, T., Oya, T., Monden, K., Nagae, A. & Nakagawa, T. (2021) A cellophane-
763 supported Arabidopsis culture for seamless transfer between different media is useful for
764 studying various nitrogen responses. *Soil Sci. Plant Nutr.*, **67**(3), 277–282.
765
766 Higuchi, M., Pischke, M.S., Mähönen, A.P., Miyawaki, K., Hashimoto, Y., Seki, M. *et*
767 *al*. (2004) In planta functions of the Arabidopsis cytokinin receptor family. *Proc. Natl.*
768 *Acad. Sci. U S A*, **101**(23), 8821–8826.
769
770 Hirose, N., Takei, K., Kuroha, T., Kamada-Nobusada, T., Hayashi, H. & Sakakibara, H.
771 (2008) Regulation of cytokinin biosynthesis, compartmentalization and translocation. *J.*
772 *Exp. Bot.*, **59**(1), 75–83.
773
774 Hošek, P., Hoyerová, K., Kiran, N.S., Dobrev, P.I., Zahajská, L., Filepová, R. *et al*. (2020)
775 Distinct metabolism of N-glucosides of isopentenyladenine and trans-zeatin determines
776 cytokinin metabolic spectrum in Arabidopsis. *New Phytol.*, **225**(6), 2423–2438.
777
778 Hutchison, C.E. & Kieber, J.J. (2002) Cytokinin signaling in Arabidopsis. *Plant Cell*,
779 **14**(suppl_1), S47–S59.
780
781 Inoue, T., Higuchi, M., Hashimoto, Y., Seki, M., Kobayashi, M., Kato, T. *et al*. (2001)
782 Identification of CRE1 as a cytokinin receptor from Arabidopsis. *Nature*, **409**(6823),
783 1060–1063.
784

785 Jin, S.H., Ma, X.M., Kojima, M., Sakakibara, H., Wang, Y.W. & Hou, B.K. (2013)
786 Overexpression of glucosyltransferase UGT85A1 influences trans-zeatin homeostasis
787 and trans-zeatin responses likely through O-glucosylation. *Planta*, **237**(4), 991–999.
788
789 Kiba, T., Takei, K., Kojima, M. & Sakakibara, H. (2013) Side-chain modification of
790 cytokinins controls shoot growth in Arabidopsis. *Dev. Cell*, **27**(4), 452–461.
791
792 Kiba, T., Inaba, J., Kudo, T., Ueda, N., Konishi, M., Mitsuda, N. *et al*. (2018) Repression
793 of nitrogen starvation responses by members of the Arabidopsis GARP-type transcription
794 factor NIGT1/HRS1 subfamily. *Plant Cell*, **30**(4), 925–945.
795
796 Kim, H.J., Ryu, H., Hong, S.H., Woo, H.R., Lim, P.O., Lee, I.C. *et al*. (2006) Cytokinin-
797 mediated control of leaf longevity by AHK3 through phosphorylation of ARR2 in
798 Arabidopsis. *Proc. Natl. Acad. Sci. U S A*, **103**(3), 814–819.
799
800 Ko, D., Kang, J., Kiba, T., Park, J., Kojima, M., Do, J. *et al*. (2014) Arabidopsis ABCG14
801 is essential for the root-to-shoot translocation of cytokinin. *Proc. Natl. Acad. Sci. USA*,
802 **111**(19), 7150–7155.
803
804 Kojima, M., Kamada-Nobusada, T., Komatsu, H., Takei, K., Kuroha, T., Mizutani, M. *et*
805 *al*. (2009) Highly sensitive and high-throughput analysis of plant hormones using MS-
806 probe modification and liquid chromatography–tandem mass spectrometry: an
807 application for hormone profiling in Oryza sativa. *Plant Cell Physiol.*, **50**(7), 1201–1214.
808

809 Kubiasová, K., Montesinos, J.C., Šamajová, O., Nisler, J., Mik, V., Semerádová, H. *et al*.
810 (2020) Cytokinin fluoroprobe reveals multiple sites of cytokinin perception at plasma
811 membrane and endoplasmic reticulum. *Nat. Commun.*, **11**(1), 4285.
812
813 Kurakawa, T., Ueda, N., Maekawa, M., Kobayashi, K., Kojima, M., Nagato, Y. *et al*.
814 (2007) Direct control of shoot meristem activity by a cytokinin-activating enzyme.
815 *Nature*, **445**(7128), 652–655.
816
817 Kuroha, T., Tokunaga, H., Kojima, M., Ueda, N., Ishida, T., Nagawa, S. *et al*. (2009)
818 Functional analyses of LONELY GUY cytokinin-activating enzymes reveal the
819 importance of the direct activation pathway in Arabidopsis. *Plant Cell*, **21**(10), 3152–
820 3169.
821
822 Landrein, B., Formosa-Jordan, P., Malivert, A., Schuster, C., Melnyk, C.W., Yang, W. *et*
823 *al*. (2018) Nitrate modulates stem cell dynamics in Arabidopsis shoot meristems through
824 cytokinins. *Proc. Natl. Acad. Sci. U S A*, **115**(6), 1382–1387.
825
826 Langmead, B., Trapnell, C., Pop, M. & Salzberg, S.L. (2009) Ultrafast and memory-
827 efficient alignment of short DNA sequences to the human genome. *Genome Biol.*, **10**(3),
828 R25.
829
830 Liu, K.H., Liu, M., Lin, Z., Wang, Z.F., Chen, B., Liu, C. *et al*. (2022) NIN-like protein
831 7 transcription factor is a plant nitrate sensor. *Science*, **377**(6613), 1419–1425.
832

833 Loperfido, D., Zumajo-Cardona, C., Commisso, M., Guzzo, F., Ambrose, B., Colombo,
834 L. *et al*. (2025) The role of cytokinin receptors in Arabidopsis thaliana seed development
835 and how they affect the metabolomic profile. *Planta*, **262**(59).
836
837 Maeda, Y., Konishi, M., Kiba, T., Sakuraba, Y., Sawaki, N., Kurai, T. *et al*. (2018) A
838 NIGT1-centred transcriptional cascade regulates nitrate signalling and incorporates
839 phosphorus starvation signals in Arabidopsis. *Nat. Commun.*, **9**(1), 1376.
840
841 Matsumoto-Kitano, M., Kusumoto, T., Tarkowski, P., Kinoshita-Tsujimura, K.,
842 Václavíková, K., Miyawaki, K. *et al*. (2008) Cytokinins are central regulators of cambial
843 activity. *Proc. Natl. Acad. Sci. U S A*, **105**(50), 20027–20031.
844
845 Miyawaki, K., Matsumoto-Kitano, M. & Kakimoto, T. (2004) Expression of cytokinin
846 biosynthetic isopentyltransferase genes in Arabidopsis: tissue specificity and regulation
847 by auxin, cytokinin, and nitrate. *Plant J.*, **37**(1), 128–138.
848
849 Miyawaki, K., Tarkowski, P., Matsumoto-Kitano, M., Kato, T., Sato, S., Tarkowska, D.
850 *et al*. (2006) Roles of Arabidopsis ATP/ADP isopentenyltransferases and tRNA
851 isopentenyltransferases in cytokinin biosynthesis. *Proc. Natl. Acad. Sci. U S A*, **103**(44),
852 16598–16603.
853
854 Monden, K., Kojima, M., Takebayashi, Y., Suzuki, T., Nakagawa, T., Sakakibara, H. *et*
855 *al*. (2022) Root-specific reduction of cytokinin perception enhances shoot growth in
856 Arabidopsis thaliana. *Plant Cell Physiol.*, **63**(4), 484–493.

857

858 Müller, B. & Sheen, J. (2007) Arabidopsis cytokinin signaling pathway. *Sci. STKE*, **407**,
859 cm5.

860

861 Nam, Y.J., Tran, L.S., Kojima, M., Sakakibara, H., Nishiyama, R. & Shin, R. (2012)
862 Regulatory roles of cytokinins and cytokinin signaling in response to potassium
863 deficiency in Arabidopsis. *PLoS One*, **7**(10), e47797.

864

865 Niemann, M.C.E., Weber, H., Hluska, T., Leonte, G., Anderson, S.M., Novak, O. *et al*.
866 (2018) The cytokinin oxidase/dehydrogenase CKX1 is a membrane-bound protein
867 requiring homooligomerization in the endoplasmic reticulum for its cellular activity.
868 *Plant Physiol.*, **176**(3), 2024–2039.

869

870 Notaguchi, M., Higashiyama, T. & Suzuki, T. (2015) Identification of mRNAs that move
871 over long distances using an RNA-Seq analysis of Arabidopsis/Nicotiana benthamiana
872 heterografts. *Plant Cell Physiol.*, **56**(2), 311–321.

873

874 Osugi, A., Kojima, M., Takebayashi, Y., Ueda, N., Kiba, T. & Sakakibara, H. (2017)
875 Systemic transport of trans-zeatin and its precursor have differing roles in Arabidopsis
876 shoots. *Nat. Plants*, **3**, 17112.

877

878 Riefler, M., Novak, O., Strnad, M. & Schmülling, T. (2006) Arabidopsis cytokinin
879 receptor mutants reveal functions in shoot growth, leaf senescence, seed size, germination,
880 root development, and cytokinin metabolism. *Plant Cell*, **18**(1), 40–54.

881

882 Romanov, G.A., Lomin, S.N. & Schmülling, T. (2006) Biochemical characteristics and
883 ligand-binding properties of Arabidopsis cytokinin receptor AHK3 compared to
884 CRE1/AHK4 as revealed by a direct binding assay. *J. Exp. Bot.*, **57**(15), 4051–4058.

885

886 Sakakibara, H., Suzuki, M., Takei, K., Deji, A., Taniguchi, M. & Sugiyama, T. (1998) A
887 response‐regulator homologue possibly involved in nitrogen signal transduction
888 mediated by cytokinin in maize. *Plant J.*, **14**, 337‐344.

889

890 Sakakibara, H., Takei, K. & Hirose, N. (2006) Interactions between nitrogen and
891 cytokinin in the regulation of metabolism and development. *Trends Plant Sci.*, **11**, 440–
892 448.

893

894 Sakakibara, H. (2021) Cytokinin biosynthesis and transport for systemic nitrogen
895 signaling. *Plant J.*, **105**(2), 421–430.

896

897 Sakakibara, H. (2025) Five unaddressed questions about cytokinin biosynthesis. *J. Exp.*
898 *Bot.*, **76**(7), 1941–1949.

899

900 Schmülling, T., Werner, T., Riefler, M., Krupková, E. & Bartrina y Manns, I. (2003)
901 Structure and function of cytokinin oxidase/dehydrogenase genes of maize, rice,
902 Arabidopsis and other species. *J. Plant Res.*, **116**, 241–252.

903

904 Spichal, L., Rakova, N.Y., Riefler, M., Mizuno, T., Romanov, G.A., Strnad, M. *et al*.
905 (2004) Two cytokinin receptors of Arabidopsis thaliana, CRE1/AHK4 and AHK3, differ
906 in their ligand specificity in a bacterial assay. *Plant Cell Physiol.*, **45**(9), 1299–1305.
907
908 Stolz, A., Riefler, M., Lomin, S.N., Achazi, K., Romanov, G.A. & Schmülling, T. (2011)
909 The specificity of cytokinin signalling in Arabidopsis thaliana is mediated by differing
910 ligand affinities and expression profiles of the receptors. *Plant J.*, **67**(1), 157–168.
911
912 Takei, K., Sakakibara, H. & Sugiyama, T. (2001a) Identification of genes encoding
913 adenylate isopentenyltransferase, a cytokinin biosynthesis enzyme, in Arabidopsis
914 thaliana. *J. Biol. Chem.*, **276**(28), 26405–26410.
915
916 Takei, K., Sakakibara, H., Taniguchi, M. & Sugiyama, T. (2001b) Nitrogen-dependent
917 accumulation of cytokinins in root and the translocation to leaf: implication of cytokinin
918 species that induces gene expression of maize response regulator. *Plant Cell Physiol.*,
919 **42**(1), 85–93.
920
921 Takei, K., Yamaya, T. & Sakakibara, H. (2004a) Arabidopsis CYP735A1 and
922 CYP735A2 encode cytokinin hydroxylases that catalyze the biosynthesis of trans-zeatin.
923 *J. Biol. Chem.*, **279**(40), 41866–41872.
924
925 Takei, K., Ueda, N., Aoki, K., Kuromori, T., Hirayama, T., Shinozaki, K. *et al*. (2004b)
926 AtIPT3 is a key determinant of nitrate-dependent cytokinin biosynthesis in Arabidopsis.
927 *Plant Cell Physiol.*, **45**(8), 1053–1062.

928

929 To, J.P.C., Haberer, G., Ferreira, F.J., Deruère, J., Mason, M.G., Schaller, G.E. *et al*.
930 (2004) Type-A ARRs are partially redundant negative regulators of cytokinin signaling
931 in Arabidopsis. *Plant Cell*, **16**(3), 658–671.

932

933 Wang, J., Ma, X.M., Kojima, M., Sakakibara, H. & Hou, B.K. (2011) N-
934 Glucosyltransferase UGT76C2 is involved in cytokinin homeostasis and cytokinin
935 response in Arabidopsis thaliana. *Plant Cell Physiol.*, **52**(12), 2200–2213.

936

937 Wang, J., Ma, X.M., Kojima, M., Sakakibara, H. & Hou, B.K. (2013) Glucosyltransferase
938 UGT76C1 finely modulates cytokinin responses via cytokinin N-glucosylation in
939 Arabidopsis thaliana. *Plant Physiol. Biochem.*, **65**, 9–16.

940

941 Werner, T., Motyka, V., Strnad, M. & Schmülling, T. (2001) Regulation of plant growth
942 by cytokinin. *Proc. Natl. Acad. Sci. USA*, **98**(18), 10487–10492.

943

944 Werner, T., Motyka, V., Laucou, V., Smets, R., Van Onckelen, H. & Schmülling, T.
945 (2003) Cytokinin-deficient transgenic Arabidopsis plants show multiple developmental
946 alterations indicating opposite functions of cytokinins in the regulation of shoot and root
947 meristem activity. *Plant Cell*, **15**(11), 2532–2550.

948

949 Werner, T., Köllmer, I., Bartrina, I., Holst, K. & Schmülling, T. (2006) New insights into
950 the biology of cytokinin degradation. *Plant Biol.*, **8**(3), 371–381.

951

952 Wulfetange, K., Lomin, S.N., Romanov, G.A., Stolz, A., Heyl, A. & Schmülling, T.
953 (2011) The cytokinin receptors of Arabidopsis are located mainly to the endoplasmic
954 reticulum. *Plant Physiol.*, **156**(4), 1808–1818.
955
956 Zhang, K., Novak, O., Wei, Z., Gou, M., Zhang, X., Yu, Y. *et al*. (2014) Arabidopsis
957 ABCG14 protein controls the acropetal translocation of root-synthesized cytokinins. *Nat*
958 *Commun.*, **5**(1), 3274.
959
960 Zhao, J., Ding, B., Zhu, E., Deng, X., Zhang, M., Zhang, P. *et al*. (2021) Phloem
961 unloading via the apoplastic pathway is essential for shoot distribution of root-
962 synthesized cytokinins. *Plant Physiol.*, **186**(4), 2111–2123.
963
964 Zhao, J., Deng, X., Qian, J., Liu, T., Ju, M., Li, J. *et al*. (2023) Arabidopsis ABCG14
965 forms a homodimeric transporter for multiple cytokinins and mediates long-distance
966 transport of isopentenyladenine-type cytokinins. *Plant Commun.*, **4**(2), 100468.
967
968 Zürcher, E., Tavor-Deslex, D., Lituiev, D., Enkerli, K., Tarr, P.T. & Müller, B. (2013) A
969 robust and sensitive synthetic sensor to monitor the transcriptional output of the cytokinin
970 signaling network in planta. *Plant Physiol.*, **161**(3), 1066–1075.
971
972 **FIGURE LEGENDS**
973 **Figure 1. Effects of root-specific CK receptor deficiency on shoot growth in medium.**
974 (A) Representative shoots of grafted plants. Scale bars = 5 mm. (B–D) Shoot fresh weight
975 (B), leaf blade area (C), and leaf number (D) of grafted plants. Data pooled from two

976 independent grafting experiments are shown as mean ± SD (n = 12). Different lowercase
977 letters indicate significant differences, as determined via Tukey–Kramer test ($P < 0.05$).
978 Numbers on graphs show mean values relative to WT/WT (set = 1). Grafted plants are
979 denoted as "scion line/rootstock line." WT, Col-0; *a2*, *ahk2-5*; *a3*, *ahk3-7*; *a4*, *cre1-2*;
980 *a23*, *ahk2-5 ahk3-7*; *a24*, *ahk2-5 cre1-2*; *a34*, *ahk3-7 cre1-2*.
981
982 **Figure 2. Effects of root-specific CK receptor deficiency on root CK concentration.**
983 (A–B) Root concentrations of active form iP and *t*Z and their precursors (A), and inactive
984 form iP- and *t*Z-type CKs (B) in grafted plants. Data are pooled from three independent
985 grafting experiments and are reported as mean ± SD (n = 3). Different lowercase letters
986 indicate significant differences, as determined via Tukey–Kramer test ($P < 0.05$). Grafted
987 plants are denoted as "scion line/rootstock line." WT, Col-0; *a2*, *ahk2-5*; *a3*, *ahk3-7*; *a4*,
988 *cre1-2*; FW, fresh weight; *t*Z, *trans*-zeatin; iP, N^6-(Δ^2-isopentenyl) adenine; iP and their
989 precursors = sum of iP, iPR, and iPRPs; inactive form iP-type CKs = sum of iP7G and
990 iP9G; *t*Z and their precursors = sum of *t*Z, *t*ZR, and *t*ZRPs; inactive form *t*Z-type CKs =
991 sum of *t*Z7G, *t*Z9G, *t*ZOG, and *t*ZROG.
992
993 **Figure 3. Effects of root-specific CK receptor deficiency on the root transcriptome.**
994 (A) Volcano plots of DEGs between WT/WT and WT/*ahk2*, WT/*ahk3*, or WT/*ahk4* roots.
995 DEG analysis was performed with RNAseqChef (Etoh et al., 2023) using edgeR, applying
996 a 1.5-fold change threshold and FDR cutoff of 0.15 (all other parameters default). x-axis:
997 $\log_2$ fold change ($\log_2$ FC); y-axis: $-\log_{10}$ adjusted p-value (padj). Each dot represents a
998 single gene. Red, blue, and grey indicate upregulated, downregulated, and non-significant
999 genes, respectively. Log_2 FC was limited to –4 to 4 and padj to ≦50. Full-range volcano

1000 plots are provided in Supplementary Fig. S4. (B) Mean normalized transcript levels of
1001 CK-inducible and CK-repressible genes (mean ± SD). Gene list obtained from Bhargava
1002 *et al*. (2013). (C) Transcriptional changes in CK biosynthesis and inactivation genes,
1003 visualized as heatmaps with MORPHEUS (https://software.broadinstitute.org/morpheus)
1004 based on $\log_2$-transformed ratios of each graft to WT/WT mean RPM. Color scale: blue
1005 (minimum) to yellow (maximum) per row. (D) Root expression of *CKX4* in grafted plants
1006 by qRT-PCR. Relative transcript levels were normalized to the WT/WT root mean (set =
1007 1) and $\log_2$-transformed. Data pooled from two independent grafting experiments are
1008 shown as mean ± SD (n = 6). Different lowercase letters indicate significant differences,
1009 as determined via Tukey–Kramer test ($P < 0.05$). Grafted plants are denoted as "scion
1010 line/rootstock line." WT, Col-0; *a2*, *ahk2-5*; *a3*, *ahk3-7*; *a4*, *cre1-2*; FC, fold change.
1011
1012 **Figure 4. Effects of root-specific CK receptor deficiency on CK concentration of**
1013 **xylem sap.** (A–B) Xylem sap concentrations of iP- and *t*Z-type CKs (A) and of *t*Z, *t*ZR,
1014 and *t*ZRPs (B) in grafted plants. Data pooled from three independent grafting experiments
1015 are reported as mean ± SD (n = 3). Different lowercase letters indicate significant
1016 differences, as determined via Tukey–Kramer test ($P < 0.05$). Grafted plants are denoted
1017 as "scion line/rootstock line." WT, Col-0; *a2*, *ahk2-5*; *a3*, *ahk3-7*; *a4*, *cre1-2*; *t*Z, *trans*-
1018 zeatin; *t*ZR, *t*Z-riboside; *t*ZRPs, *t*ZR 5′-phosphates; iP-type CKs = sum of iPR, iPRPs,
1019 and iP7G; *t*Z-type CKs = sum of *t*Z, *t*ZR, *t*ZRPs, *t*Z7G, *t*Z9G, and *t*ZOG.
1020
1021 **Figure 5. Effects of root-specific CK receptor deficiency on the shoot transcriptome.**
1022 (A) Volcano plots of DEGs between WT/WT and WT/*ahk2*, WT/*ahk3*, or WT/*ahk4*
1023 shoots. DEG analysis was performed with RNAseqChef (Etoh et al., 2023) using edgeR,

1024 applying a 1.5-fold change threshold and FDR cutoff of 0.15 (default parameters
1025 otherwise). x-axis: $\log_2$ fold change ($\log_2$ FC); y-axis: $-\log_{10}$ adjusted p-value (padj). Each
1026 dot represents one gene; red, blue, and grey indicate upregulated, downregulated, and
1027 non-significant genes, respectively. Log_2 FC values were limited to –4 to 4 and padj
1028 values to ≦5. (B) Lollipop plots showing GO enrichment analysis from the 163 genes
1029 upregulated in WT/*ahk3* shoots, generated with ShinyGO (Ge et al., 2020) using default
1030 settings for biological process terms. (C) Heatmaps of transcriptional changes in type-A
1031 *ARR* genes, visualized with MORPHEUS (https://software.broadinstitute.org/morpheus)
1032 based on $\log_2$-transformed ratios of each graft to the WT/WT mean RPM. Color scale:
1033 blue (minimum) to yellow (maximum) per row. (D) Shoot expression of *ARR5*
1034 determined by qRT-PCR. Values were normalized to the WT/WT shoot mean (set = 1)
1035 and $\log_2$-transformed. Data pooled from two independent grafting experiments are
1036 reported as mean ± SD (n = 6). Different lowercase letters indicate significant differences,
1037 as determined via Tukey–Kramer test ($P < 0.05$). Grafted plants are denoted as "scion
1038 line/rootstock line." WT, Col-0; *a2*, *ahk2-5*; *a3*, *ahk3-7*; *a4*, *cre1-2*; FC, fold change.
1039
1040 **Figure 6. Effects of root-specific *AHK3* deficiency on shoot growth via CK signaling.**
1041 (A–E) Shoot fresh weight and leaf blade area in grafted plants: (A) WT/WT, WT/*ahk3*,
1042 WT/*abcg14*, and WT/*ahk3 abcg14*; (B) WT/WT, WT/*ahk3*, WT/*cypDM*, and WT/*ahk3*
1043 *cypDM*; (C) WT/WT, WT/*ahk3*, *ahk2*/*ahk3*, *ahk3*/*ahk3*, and *ahk4*/*ahk3*; (D) WT/WT,
1044 WT/*ahk3*, *ahk23*/*ahk3*, *ahk24*/*ahk3*, and *ahk34*/*ahk3*; (E) *TCSn:GFP*/WT and
1045 *TCSn:GFP*/*ahk3*. (F) Representative fluorescent image of the adaxial side of the sixth
1046 true leaf in grafted plants. Green = GFP; red = autofluorescence. Scale bars = 1 mm. GFP
1047 intensity was quantified with ImageJ as the mean signal in the region marked by a white

1048 dashed box. (G) Epidermal cell size and number on the abaxial side of the fifth true leaf.
1049 Data pooled from two independent grafting experiments are reported as mean ± SD (n =
1050 12 (A–E), 11 (F), or 6 (G)). Different lowercase letters indicate significant differences,
1051 as determined via Tukey–Kramer test ($P < 0.05$). Asterisks indicate significant
1052 differences (**$P < 0.01$, ***$P < 0.001$, Welch's *t*-test). Graph numbers show mean values
1053 relative to WT/WT (set = 1). Grafted plants are denoted as "scion line/rootstock line."
1054 WT, Col-0; *a2*, *ahk2-5*; *a3*, *ahk3-7*; *a4*, *cre1-2*; *a23*, *ahk2-5 ahk3-7*; *a24*, *ahk2-5 cre1-2*;
1055 *a34*, *ahk3-7 cre1-2*; *g14*, *abcg14*; *DM*, *cyp735a1-2 cyp735a2-2*; *a3g14*, *ahk3-7 abcg14*;
1056 *a3DM*, *ahk3-7 cyp735a1-2 cyp735a2-2*; *TCS*, *TCSn:GFP*; ns, not significant.
1057
1058 **Figure 7. Effects of root-specific *AHK3* or *CKX4* deficiency on shoot growth in**
1059 **response to nitrate signaling.** (A, B, E) Shoot fresh weight and leaf blade area of grafted
1060 plants 5 days after transfer from 5 mM NH_4^+ medium to either 5 mM NH_4^+ + 0.5 mM
1061 KNO_3 or 5 mM NH_4^+ + 0.5 mM KCl: (A) WT/WT and WT/*ahk3*; (B) WT/WT, WT/*ahk3*,
1062 WT/*abcg14*, and WT/*ahk3 abcg14*; (E) WT/WT, WT/*ckx4-1*, and WT/*ckx4-2*. (C) Root
1063 expression of *IPT3*, *IPT7*, *CYP735A1*, *CYP735A2*, *CKX1*, *CKX3*, *CKX4*, *CKX5*, *CKX6*,
1064 *CKX7*, *UGT76C1*, *UGT76C2*, and *UGT85A1* 4 hours after transfer. Heatmaps were
1065 generated with MORPHEUS (https://software.broadinstitute.org/morpheus) from $\log_2$
1066 fold change values relative to WT/WT under 5 mM NH_4^+ + 0.5 mM KCl (set = 1). Color
1067 scale: blue (minimum) to yellow (maximum) per row. (D) RT-PCR analysis of *CKX4* in
1068 WT, *ckx4-1*, and *ckx4-2* seedlings grown 7 days on 1/2 MS medium. *TIP41* was the
1069 control. Primers are listed in Supplementary Table S8. Data are shown as mean ± SD with
1070 replicates as follows: (A) n = 18, two replicates; (B) n = 18, three replicates; (C) n = 6,
1071 two replicates; (E) n = 24, four replicates. Different lowercase letters indicate significant

1072 differences, as determined via Tukey–Kramer test ($P < 0.05$). Graph numbers indicate
1073 mean values relative to WT/WT under 5 mM NH_4^+ + 0.5 mM KCl (set = 1). Grafted
1074 plants are denoted as "scion line/rootstock line." WT, Col-0; *a3*, *ahk3-7*; *g14*, *abcg14*;
1075 *a3g14*, *ahk3-7 abcg14*; *c4-1*, *ckx4-1*; *c4-2*, *ckx4-2*; ns, not significant; KCl, 5 mM NH_4^+
1076 + 0.5 mM KCl; KNO_3, 5 mM NH_4^+ + 0.5 mM KNO_3.

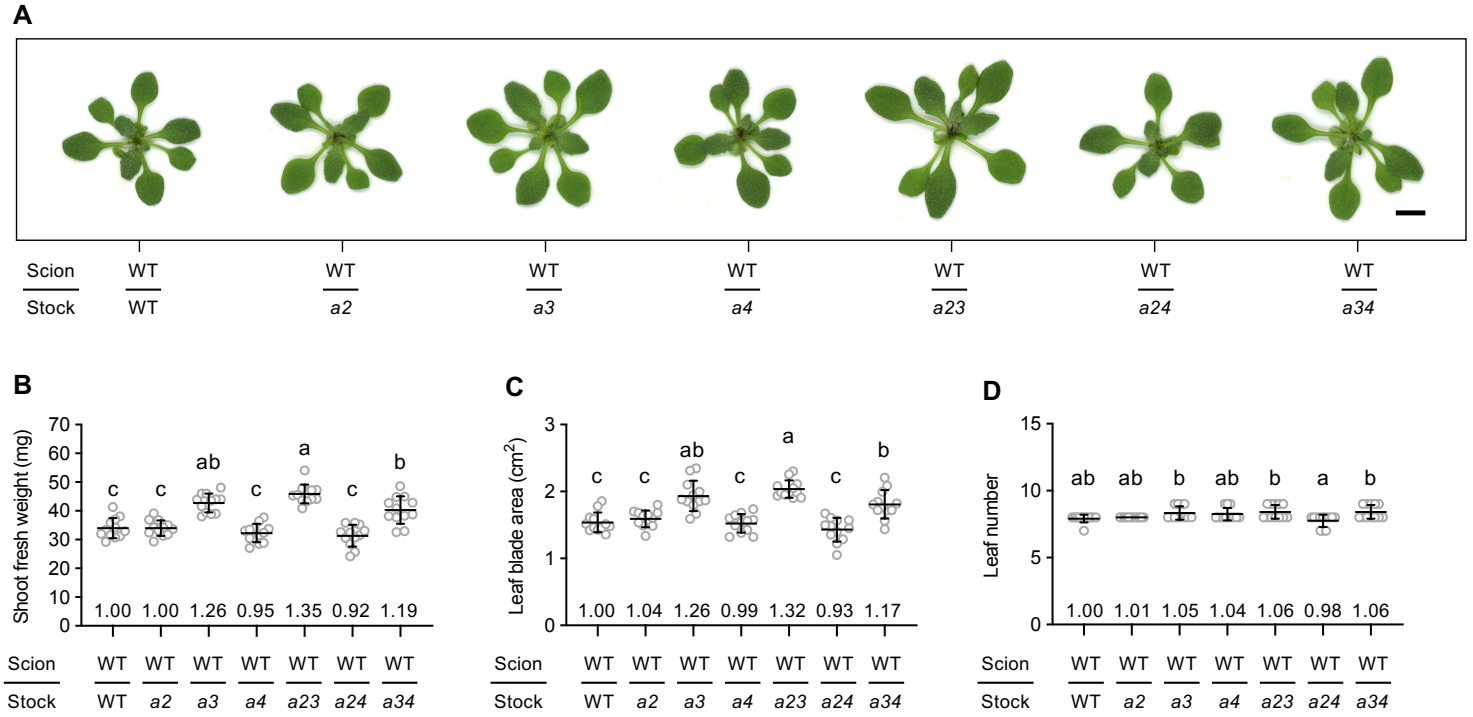

Figure 1. Effects of root-specific CK receptor deficiency on shoot growth in medium. (A) Representative shoots of grafted plants. Scale bars = 5 mm. (B–D) Shoot fresh weight (B), leaf blade area (C), and leaf number (D) of grafted plants. Data pooled from two independent grafting experiments are shown as mean ± SD (n = 12). Different lowercase letters indicate significant differences, as determined via Tukey–Kramer test ($P < 0.05$). Numbers on graphs show mean values relative to WT/WT (set = 1). Grafted plants are denoted as "scion line/rootstock line." WT, Col-0; *a2*, *ahk2-5*; *a3*, *ahk3-7*; *a4*, *cre1-2*; *a23*, *ahk2-5 ahk3-7*; *a24*, *ahk2-5 cre1-2*; *a34*, *ahk3-7 cre1-2*.

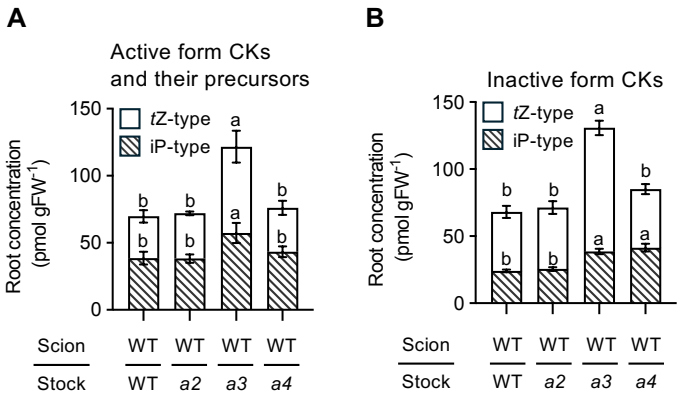

Figure 2. Effects of root-specific CK receptor deficiency on root CK concentration. (A–B) Root concentrations of active form iP and *t*Z and their precursors (A), and inactive form iP- and *t*Z-type CKs (B) in grafted plants. Data are pooled from three independent grafting experiments and are reported as mean ± SD (n = 3). Different lowercase letters indicate significant differences, as determined via Tukey–Kramer test ($P < 0.05$). Grafted plants are denoted as "scion line/rootstock line." WT, Col-0; *a2*, *ahk2-5*; *a3*, *ahk3-7*; *a4*, *cre1-2*; FW, fresh weight; *t*Z, *trans*-zeatin; iP, N^6-(Δ^2-isopentenyl) adenine; iP and their precursors = sum of iP, iPR, and iPRPs; inactive form iP-type CKs = sum of iP7G and iP9G; *t*Z and their precursors = sum of *t*Z, *t*ZR, and *t*ZRPs; inactive form *t*Z-type CKs = sum of *t*Z7G, *t*Z9G, *t*ZOG, and *t*ZROG.

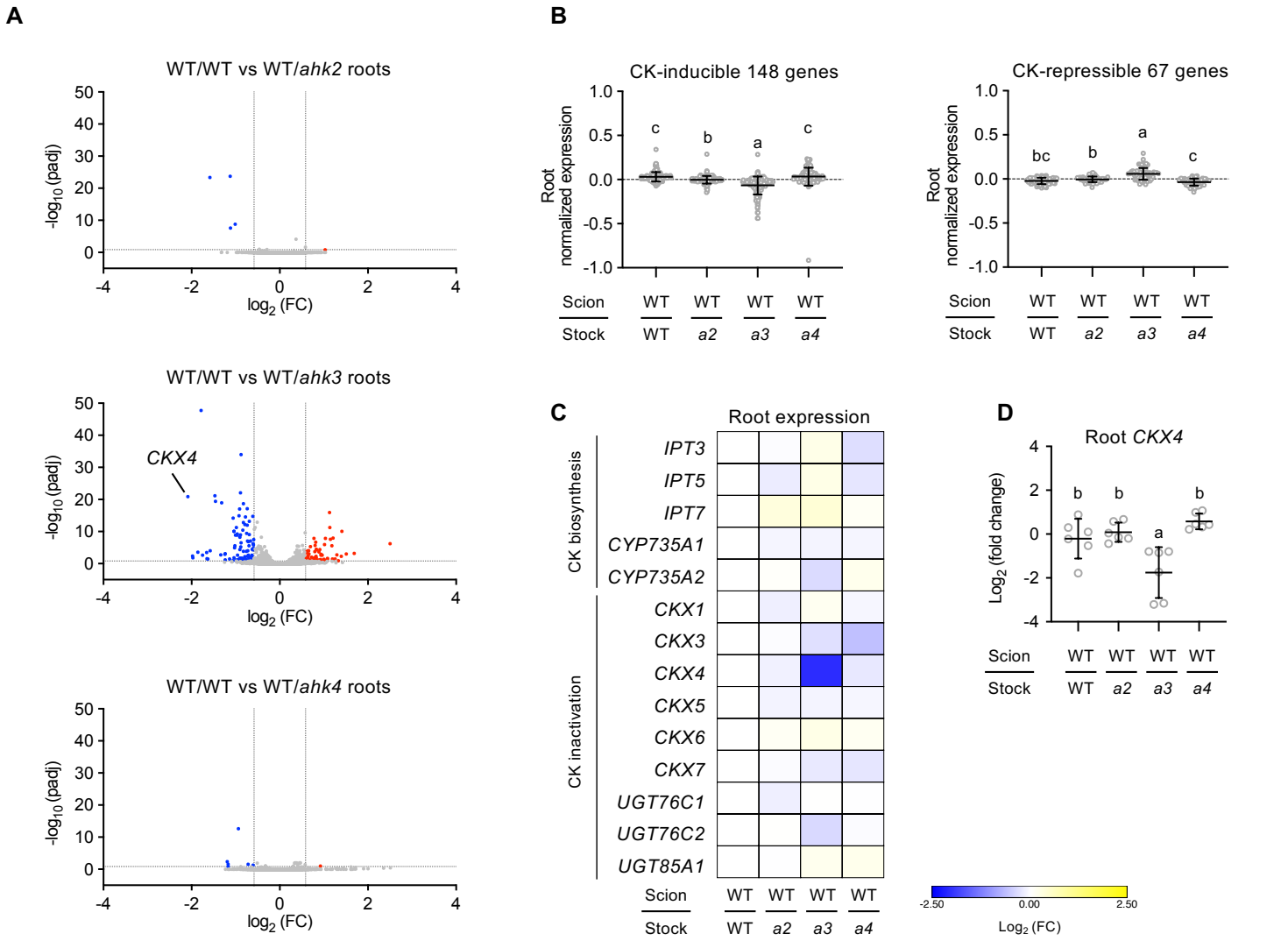

Figure 3. Effects of root-specific CK receptor deficiency on the root transcriptome. (A) Volcano plots of DEGs between WT/WT and WT/*ahk2*, WT/*ahk3*, or WT/*ahk4* roots. DEG analysis was performed with RNAseqChef (Etoh et al., 2023) using edgeR, applying a 1.5-fold change threshold and FDR cutoff of 0.15 (all other parameters default). x-axis: $\log_2$ fold change ($\log_2$ FC); y-axis: $-\log_{10}$ adjusted p-value (padj). Each dot represents a single gene. Red, blue, and grey indicate upregulated, downregulated, and non-significant genes, respectively. Log_2 FC was limited to –4 to 4 and padj to ≦50. Full-range volcano plots are provided in Supplementary Fig. S4. (B) Mean normalized transcript levels of CK-inducible and CK-repressible genes (mean ± SD). Gene list obtained from Bhargava *et al.* (2013). (C) Transcriptional changes in CK biosynthesis and inactivation genes, visualized as heatmaps with MORPHEUS (https://software.broadinstitute.org/morpheus) based on $\log_2$-transformed ratios of each graft to WT/WT mean RPM. Color scale: blue (minimum) to yellow (maximum) per row. (D) Root expression of *CKX4* in grafted plants by qRT-PCR. Relative transcript levels were normalized to the WT/WT root mean (set = 1) and $\log_2$-transformed. Data pooled from two independent grafting experiments are shown as mean ± SD (n = 6). Different lowercase letters indicate significant differences, as determined via Tukey–Kramer test ($P < 0.05$). Grafted plants are denoted as "scion line/rootstock line." WT, Col-0; *a2*, *ahk2-5*; *a3*, *ahk3-7*; *a4*, *cre1-2*; FC, fold change.

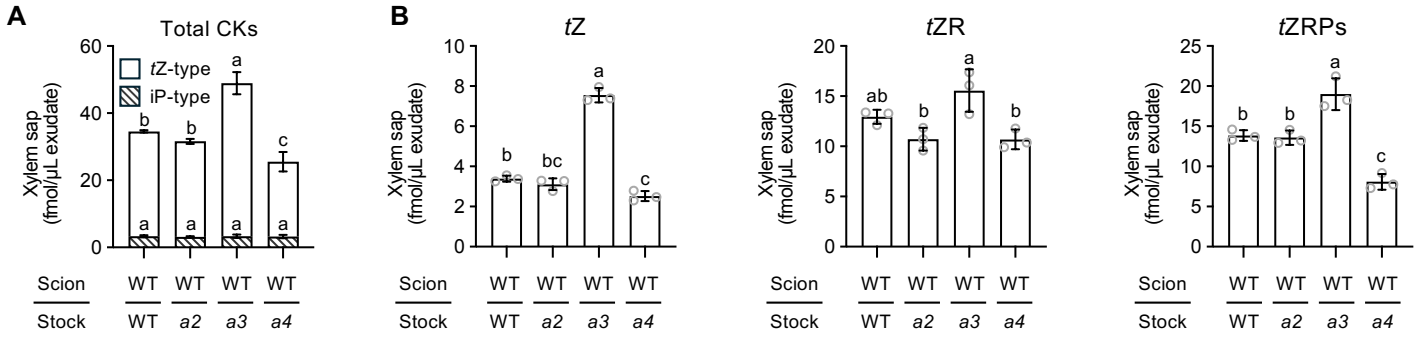

Figure 4. Effects of root-specific CK receptor deficiency on CK concentration of xylem sap. (A–B) Xylem sap concentrations of iP- and *t*Z-type CKs (A) and of *t*Z, *t*ZR, and *t*ZRPs (B) in grafted plants. Data pooled from three independent grafting experiments are reported as mean ± SD (n = 3). Different lowercase letters indicate significant differences, as determined via Tukey–Kramer test ($P < 0.05$). Grafted plants are denoted as "scion line/rootstock line." WT, Col-0; *a2*, *ahk2-5*; *a3*, *ahk3-7*; *a4*, *cre1-2*; *t*Z, *trans*-zeatin; *t*ZR, *t*Z-riboside; *t*ZRPs, *t*ZR 5′-phosphates; iP-type CKs = sum of iPR, iPRPs, and iP7G; *t*Z-type CKs = sum of *t*Z, *t*ZR, *t*ZRPs, *t*Z7G, *t*Z9G, and *t*ZOG.

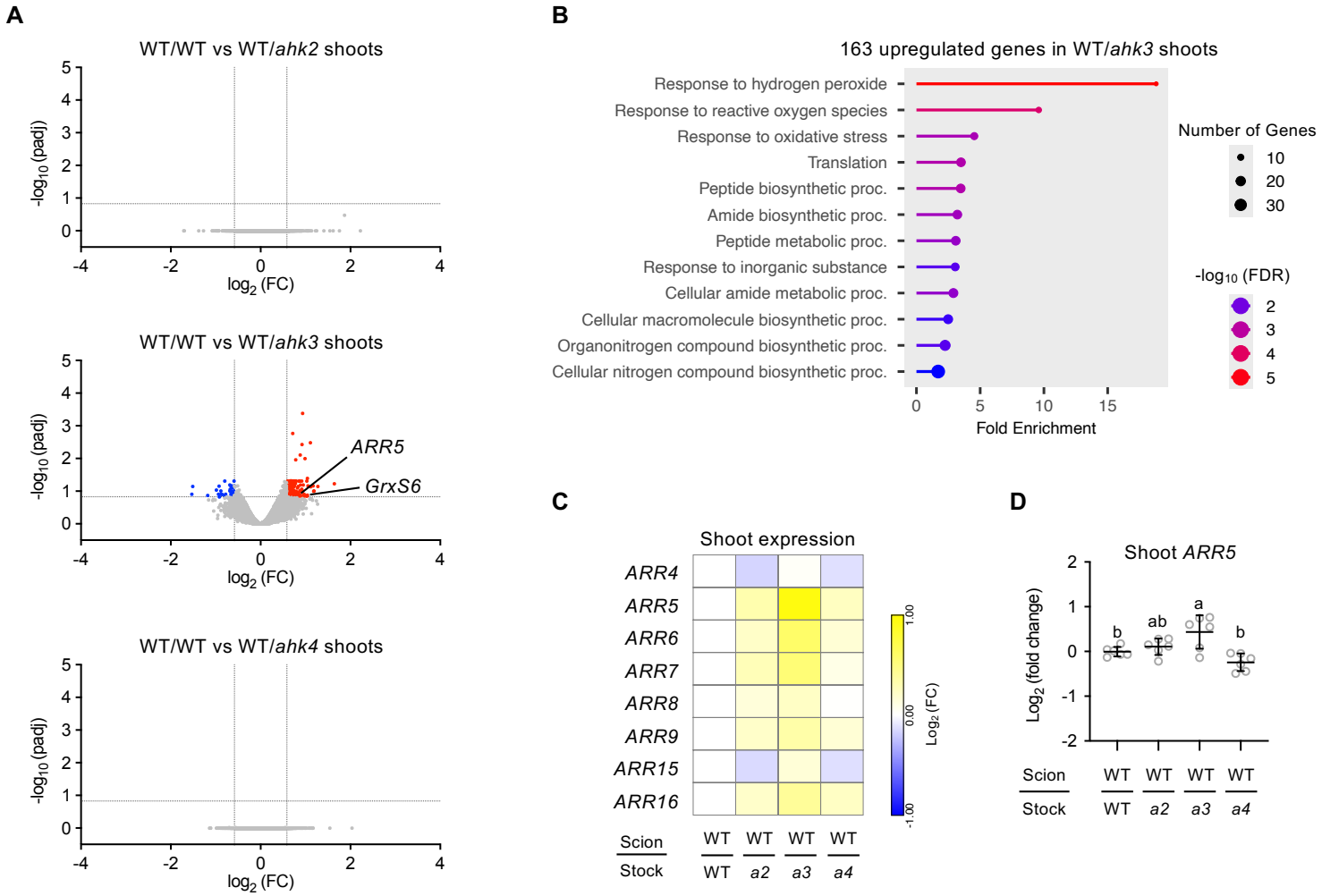

Figure 5. Effects of root-specific CK receptor deficiency on the shoot transcriptome. (A) Volcano plots of DEGs between WT/WT and WT/*ahk2*, WT/*ahk3*, or WT/*ahk4* shoots. DEG analysis was performed with RNAseqChef (Etoh et al., 2023) using edgeR, applying a 1.5-fold change threshold and FDR cutoff of 0.15 (default parameters otherwise). x-axis: $\log_2$ fold change ($\log_2$ FC); y-axis: $-\log_{10}$ adjusted p-value (padj). Each dot represents one gene; red, blue, and grey indicate upregulated, downregulated, and non-significant genes, respectively. (B) Lollipop plots showing GO enrichment analysis from the 163 genes upregulated in WT/*ahk3* shoots, generated with ShinyGO (Ge et al., 2020) using default settings for biological process terms. (C) Heatmaps of transcriptional changes in type-A *ARR* genes, visualized with MORPHEUS (https://software.broadinstitute.org/morpheus) based on $\log_2$-transformed ratios of each graft to the WT/WT mean RPM. Color scale: blue (minimum) to yellow (maximum) per row. (D) Shoot expression of *ARR5* determined by qRT-PCR. Values were normalized to the WT/WT shoot mean (set = 1) and $\log_2$-transformed. Data pooled from two independent grafting experiments are reported as mean ± SD (n = 6). Different lowercase letters indicate significant differences, as determined via Tukey–Kramer test ($P < 0.05$). Grafted plants are denoted as "scion line/rootstock line." WT, Col-0; *a2*, *ahk2-5*; *a3*, *ahk3-7*; *a4*, *cre1-2*; FC, fold change.

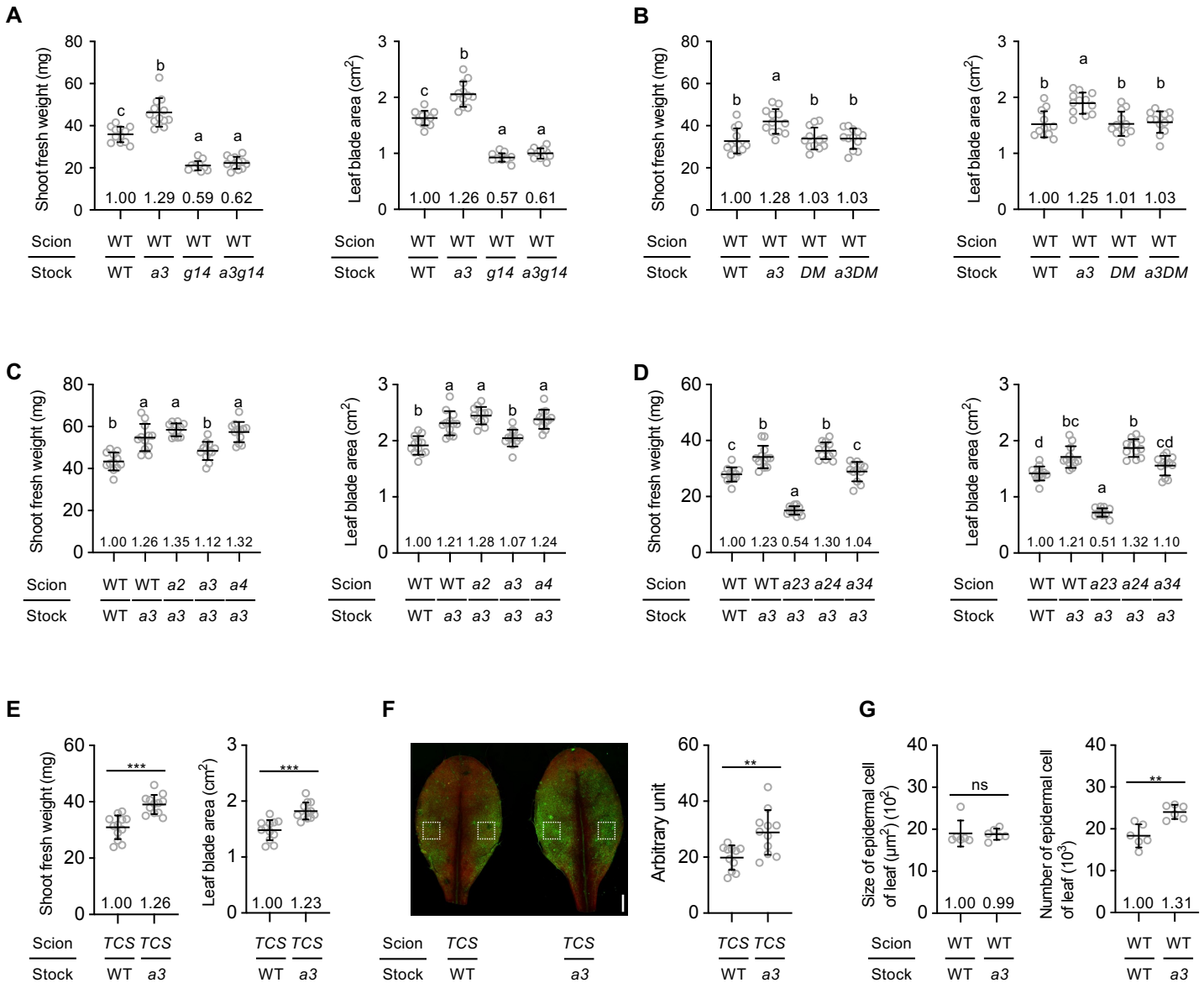

Figure 6. Effects of root-specific *AHK3* deficiency on shoot growth via CK signaling. (A–E) Shoot fresh weight and leaf blade area in grafted plants: (A) WT/WT, WT/*ahk3*, WT/*abcg14*, and WT/*ahk3 abcg14*; (B) WT/WT, WT/*ahk3*, WT/*cypDM*, and WT/*ahk3 cypDM*; (C) WT/WT, WT/*ahk3*, *ahk2*/*ahk3*, *ahk3*/*ahk3*, and *ahk4*/*ahk3*; (D) WT/WT, WT/*ahk3*, *ahk23*/*ahk3*, *ahk24*/*ahk3*, and *ahk34*/*ahk3*; (E) *TCSn:GFP*/WT and *TCSn:GFP*/*ahk3*. (F) Representative fluorescent image of the adaxial side of the sixth true leaf in grafted plants. Green = GFP; red = autofluorescence. Scale bars = 1 mm. GFP intensity was quantified with ImageJ as the mean signal in the region marked by a white dashed box. (G) Epidermal cell size and number on the abaxial side of the fifth true leaf. Data pooled from two independent grafting experiments are reported as mean ± SD (n = 12 (A–E), 11 (F), or 6 (G)). Different lowercase letters indicate significant differences, as determined via Tukey–Kramer test ($P < 0.05$). Asterisks indicate significant differences (**$P < 0.01$, ***$P < 0.001$, Welch's *t*-test). Graph numbers show mean values relative to WT/WT (set = 1). Grafted plants are denoted as "scion line/rootstock line." WT, Col-0; *a2*, *ahk2-5*; *a3*, *ahk3-7*; *a4*, *cre1-2*; *a23*, *ahk2-5 ahk3-7*; *a24*, *ahk2-5 cre1-2*; *a34*, *ahk3-7 cre1-2*; *g14*, *abcg14*; *DM*, *cyp735a1-2 cyp735a2-2*; *a3g14*, *ahk3-7 abcg14*; *a3DM*, *ahk3-7 cyp735a1-2 cyp735a2-2*; *TCS*, *TCSn:GFP*; ns, not significant.

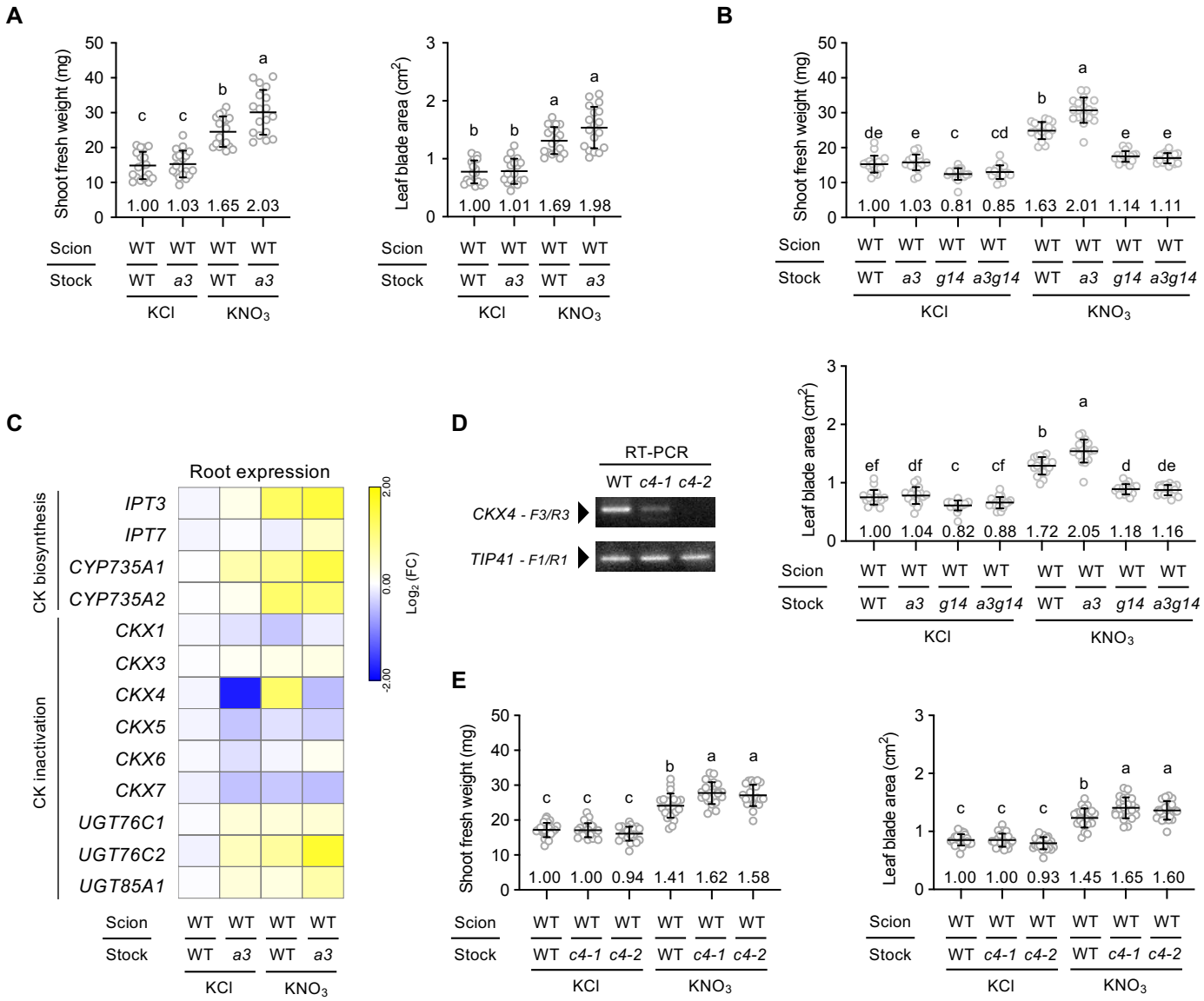

Figure 7. Effects of root-specific *AHK3* or *CKX4* deficiency on shoot growth in response to nitrate signaling. (A, B, E) Shoot fresh weight and leaf blade area of grafted plants 5 days after transfer from 5 mM NH_4^+ medium to either 5 mM NH_4^+ + 0.5 mM KNO_3 or 5 mM NH_4^+ + 0.5 mM KCl: (A) WT/WT and WT/*ahk3*; (B) WT/WT, WT/*ahk3*, WT/*abcg14*, and WT/*ahk3 abcg14*; (E) WT/WT, WT/*ckx4-1*, and WT/*ckx4-2*. (C) Root expression of *IPT3*, *IPT7*, *CYP735A1*, *CYP735A2, CKX1*, *CKX3*, *CKX4*, *CKX5*, *CKX6*, *CKX7*, *UGT76C1*, *UGT76C2*, and *UGT85A1* 4 hours after transfer. Heatmaps were generated with MORPHEUS (https://software.broadinstitute.org/morpheus) from log_2 fold change values relative to WT/WT under 5 mM NH_4^+ + 0.5 mM KCl (set = 1). Color scale: blue (minimum) to yellow (maximum) per row. (D) RT-PCR analysis of *CKX4* in WT, *ckx4-1*, and *ckx4-2* seedlings grown 7 days on 1/2 MS medium. *TIP41* was the control. Primers are listed in Supplementary Table S8. Data are shown as mean ± SD with replicates as follows: (A) n = 18, two replicates; (B) n = 18, three replicates; (C) n = 6, two replicates; (E) n = 24, four replicates. Different lowercase letters indicate significant differences, as determined via Tukey–Kramer test ($P < 0.05$). Graph numbers indicate mean values relative to WT/WT under 5 mM NH_4^+ + 0.5 mM KCl (set = 1). Grafted plants are denoted as "scion line/rootstock line." WT, Col-0; *a3*, *ahk3-7*; *g14*, *abcg14*; *a3g14*, *ahk3-7 abcg14*; *c4-1*, *ckx4-1*; *c4-2*, *ckx4-2*; ns, not significant; KCl, 5 mM NH_4^+ + 0.5 mM KCl; KNO_3, 5 mM NH_4^+ + 0.5 mM KNO_3.